

The Design of Salinity Sensor for Antarctic Research



Prepared by:

Cameron Clark

Department of Electrical Engineering
University of Cape Town

Prepared for:

Justin Pead

Department of Electrical Engineering
University of Cape Town

October 24, 2024

Submitted to the Department of Electrical Engineering at the University of Cape Town in partial fulfilment of the academic requirements for a Bachelor of Science degree in Mechatronics

Keywords: Salinity, Sensor, Conductivity, Temperature, Water, Measurement, Electronics, PCB

Declaration

1. I know that plagiarism is wrong. Plagiarism is to use another's work and pretend that it is one's own.
2. I have used the IEEE convention for citation and referencing. Each contribution to, and quotation in, this report 'The Design of Salinity Sensor for Antarctic Research' from the work(s) of other people has been attributed and has been cited and referenced. Any section taken from an internet source has been referenced to that source.
3. This report 'The Design of Salinity Sensor for Antarctic Research' is my own work and is in my own words (except where I have attributed it to others).
4. I have not paid a third party to complete my work on my behalf. My use of artificial intelligence software has been limited to giving overviews of topics, aiding with L^AT_EX commands, and aiding with making BibTeX citations of sources (specify precisely how you used AI to assist with this assignment, and then give examples of the prompts you used in your first appendix).
5. I have not allowed and will not allow anyone to copy my work with the intention of passing it off as his or her own work.
6. I acknowledge that copying someone else's assignment or essay, or part of it, is wrong, and declare that this is my own work



October 24, 2024

Cameron Clark

Date

Acknowledgements

I would like to thank my supervisor, Justin Pead, for his guidance and support throughout the project. He provided valuable insight into the design and testing of the prototype, and assistance with the writing of this report. I would also like to thank Brendon Daniels for his delicate soldering and adjustments made to the prototype.

I would like to thank my engineering friends, Si Teng Wu, Deereshan Naidoo, Kian Frassek, and Robert Dugmore for their assistance with the design and debugging of the prototype and the writing of this report.

Lastly, I would like to thank my family for their support extensive throughout my studies.

Abstract

The Antarctic ice shelves are a habitat that supports numerous unique species in and below the ice. Melting ice causes salt to be expelled, which drains into the ocean beneath, creating a mixing zone with properties that are currently being investigated. A prototype electrical conductivity-based salinometer was developed for this project to replace the current method of measuring the salinity of the mixing zone. The prototype was designed with a separate probe, which would be lowered through a hole in the ice to the ocean below, and a controller, which would request and display data from the probe. The probe utilised two types of electrodes made from gold and titanium to investigate the methods of measuring repeatable and accurate salinity measurements. Voltage sweeps and [Alternating Current \(AC\)](#) voltages could not produce accurate results as they needed further apparatus and investigations. Single voltage measurements were able to calculate salinities to within 4 [Practical Salinity Units \(PSU\)](#) of the expected value but were vulnerable to noise and other errors.

Contents

Abbreviations	vii
1 Introduction	1
1.1 Problem Statement	1
1.2 Background	1
1.3 Objectives	2
1.4 Scope & Limitations	2
1.5 Report Outline	2
2 Literature Review	3
2.1 Introduction	3
2.2 Salinity Definitions	3
2.3 Salinity Measurement Methods	4
2.3.1 Salinity from Chlorinity	4
2.3.2 Salinity from Conductivity	5
2.3.3 Salinity from Density	5
2.3.4 Salinity from Microwave Radiation	5
2.3.5 Salinity from Refractive Index	6
2.3.6 Salinity from Interferometry	6
2.3.7 Salinity from Magnetic Permeability	7
2.4 Salinity Measurement Devices using Conductivity	7
3 Theory Development	9
3.1 The Calculation of Salinity From Conductivity	9
3.2 Current Fringing in Conductive Materials	11
4 Design	12
4.1 Salinity Measurement Method	12
4.2 Conductivity Electrode Material	12
4.3 Conductivity Electrode Design	13
4.4 Resistance Measurement Method	15
4.5 Circuit Overview	15
4.6 Salinity Calculation and Display	18
4.7 Temperature and Depth Measurement	18
5 PCB Construction, Adjustments and Code	20
5.1 PCB Design	20
5.2 PCB Adjustments	21

5.3	Probe Code	22
5.4	Controller Code	23
5.5	Board-to-Board Communication	24
5.6	Probe Epoxy Casting	25
6	Salinometer Evaluation and Testing	27
6.1	Overview	27
6.2	Testing Apparatus	28
6.3	DAC Voltage Range and Accuracy	29
6.4	ADC Accuracy	29
6.5	Calibration Resistance	30
6.6	Resistance Measuring Accuracy	30
6.7	Voltage Sweep Repeatability	32
6.8	Voltage to Conductivity Mapping	35
6.9	Individual Voltage Measurements	38
6.10	AC Voltage Measurements	39
7	Conclusions	41
8	Recommendations	42
Bibliography		43
A	AI Use Screenshots	47
B	Graduate Attribute Assessment	53
C	Git Repository	54

List of Figures

2.1	Global salinity map generated using satellite data [25].	6
2.2	The schematic of a Conductivity, Temperature, Depth (CTD) probe developed by researchers at Uppsala University in Sweden which design contains (a) a temperature sensor, (b) three relatively small electrodes for pH and Cl- concentration, (c) conductivity electrodes, and (d) a strain gauge for the pressure membrane sensor. The design is $7.5 \times 3.5\text{mm}$ in size [41].	8
4.1	The gold electrode Printed Circuit Board (PCB) design.	14
4.2	A simplified representation of the resistance measuring circuit.	16
4.3	A simplified representation of the resistance measurement circuit using the gold electrodes with the fringe guard.	17
5.1	The probe PCB with the gold electrodes attached and some adjustments made	20
5.2	The controller PCB with the rotary switch caps attached	21
5.3	The flowchart for the probe code that measures salinity.	23
5.4	The flowchart for the board-to-board communication protocol denoting the four transaction types. The arrows denote the direction of the packets being sent over the Recommended Standard #485 (RS-485) link.	24
5.5	A top view of the probe casting mould, the controller and the connecting cable.	25
5.6	A side view of the probe casting mould showing the gold electrode spacers.	25
5.7	The probe after the epoxy casting process with the titanium electrodes and pressure sensor's flexible membrane attached.	26
5.8	A close-up of the titanium electrode with the copper wire attached.	26
6.1	The salinometer probe with multimeter cables attached to a test point and ground.	28
6.2	The bench multimeter used for the tests displaying a voltage reading.	28
6.3	The input voltage versus the output voltage of the Digital to Analogue Converter (DAC) with no load.	29
6.4	The input voltage versus the output voltage of the DAC with the maximum load of 100Ω	29
6.5	The voltage output by the DAC measured by a multimeter versus by the Analogue to Digital Converter (ADC).	30
6.6	The resistance measuring test.	31
6.7	The resistance measuring test using the corrected equation.	31
6.8	Voltage sweep repeatability test 1 with gold electrodes and the fringe shield, a voltage range of $0 - 2,6\text{V}$, and 50 samples taken of salt water sample of unknown salinity.	32
6.9	Voltage sweep repeatability test 2 with draining and resetting the DAC between each voltage sample.	32

6.10 Voltage sweep repeatability test 3 with 25 priming measurements taken before the actual measurement.	33
6.11 Voltage sweep repeatability test 4 with a varying number of priming measurements and the actual measurement taken as reverse voltage sweeps with 500 voltage samples.	33
6.12 Voltage sweep repeatability test 5 with a varying amount of relaxation time before each measurement was taken and 50 samples.	34
6.13 Voltage sweep repeatability test 6 with the difference between the titanium and gold electrodes.	34
6.14 Voltage sweep repeatability test 7 with 4 identical tests of 20 samples with 2s of relaxation time between measurements.	35
6.15 Voltage sweep repeatability test 8 with 4 identical tests of 20 samples with 2s of relaxation time between measurements.	35
6.16 Conductivity mapping test 1 with 4 tests using the gold electrodes and the fringe guard taken of a 34,8 PSU sample at 15,0°C.	36
6.17 Conductivity mapping test 2 with 4 tests using the titanium electrodes taken of a 34,8 PSU sample at 15,0°C.	36
6.18 Conductivity mapping test 3 with 4 tests using the gold electrodes and the fringe guard taken of a 24,4 PSU sample at 21,7°C.	36
6.19 Conductivity mapping test 4 with 4 tests using the titanium electrodes taken of a 24,4 PSU sample at 21,7°C.	36
6.20 Conductivity mapping test 5 with 4 tests using the gold electrodes and the fringe guard taken of a 29,1 PSU sample at 20,2°C.	37
6.21 Conductivity mapping test 6 with 4 tests using the titanium electrodes taken of a 29,1 PSU sample at 20,2°C.	37
6.22 The gold electrode tests of known samples with hyperbolic curves of best fit generated.	37
6.23 The titanium electrode tests of known samples with hyperbolic curves of best fit generated.	37
6.24 AC test 1 with a 4 sine waves centred at 0V.	39
6.25 AC test 1 with a 4 sine waves centred at 1,65V and 4 sine waves centred at -1,65V.	39
6.26 AC test 1 with a 4 250Hz sine waves centred at 0V on a 34,8 PSU sample.	40
6.27 AC test 1 with a 4 250Hz sine waves centred at 0V on a 24,4 PSU sample.	40
A.1 AI Use for Concept Overviews	47
A.2 AI Use for Concept Overviews	48
A.3 AI Use for Research Overview	49
A.4 AI Use for Research Overview	50
A.5 AI Use for L ^A T _E X commands and code	51
A.6 AI Use for L ^A T _E X commands and code	51
A.7 AI Use for BibTeX citations	52
A.8 AI Use for BibTeX citations	52

Abbreviations

%o Parts Per Thousand

AC Alternating Current

ADC Analogue to Digital Converter

CTD Conductivity, Temperature, Depth

DAC Digital to Analogue Converter

DC Direct Current

DMA Direct Memory Access

EMI Electromagnetic Interference

ENIG Electroless Nickel Immersion Gold

FPU Floating Point Unit

IC Integrated Circuit

LCD Liquid Crystal Display

LCR Inductance (L), Capacitance (C), Resistance (R)

LED Light Emitting Diode

PCB Printed Circuit Board

ppm parts per million

PSU Practical Salinity Units

RS-485 Recommended Standard #485

SCB System Control Block

SST Sea Surface Temperature

SYSRESETREQ System Reset Request

UART Universal Asynchronous Receiver-Transmitter

UCT University of Cape Town

USB Universal Serial Bus

Chapter 1

Introduction

1.1 Problem Statement

There are several methods and designs for measuring salinity which is commonly understood as the salt content of water. However, Antarctica's freezing temperatures and harsh conditions make it challenging for scientists to study this metric there. The current method of measuring involves capturing a water sample from the ocean beneath the ice sheet and bringing it to the surface for measurement. This process alters some water's physical properties, such as temperature and pressure, which can affect the salinity measurement. This project aims to design a device that can more accurately measure the salinity by using a probe to take measurements at various depths in the ocean.

1.2 Background

Antarctica is covered in a vast sheet of ice consisting of around 30 million cubic kilometres in volume, which is about 60% of the world's fresh water [1]. Part of the ice sheets rests on land, known as the continental ice sheet, while the rest floats on the ocean, known as the ice shelves [2]. The ice sheet supports a variety of species both above and below it, as well as an ecosystem within the ice itself [3].

The ice shelves surrounding the Antarctic continent constantly wax and wane [4], with the ice thickening during winter with water and salt accumulating from precipitation, sea spray, and ocean water freezing in direct contact with the ice [5]. When the water freezes, the salts are expelled from the mixture, creating small pockets and highly saline water channels known as brine channels. The brine channels form a habitat for several microorganisms that have adapted to the cold, harsh environment and a new habitat when they drain into the ocean below. Frigid brine and regular seawater mix beneath the ice shelves, creating a mixing zone which forms a unique environment that supports life. Scientists working with the [University of Cape Town \(UCT\)](#) are currently investigating the properties of the mixing zone, such as the water's salinity, temperature, currents, light penetration, and more.

To measure any given property, an ice core is drilled through the ice shelf down to the water's surface, and two main methods are employed to measure the brine-sea water mixture. Either a probe is lowered into the water through the ice core hole, allowing measurements to be taken at multiple depths, or a sample of the water is captured by lowering an open canister known as a Niskin bottle into the water, closing it at the desired depth, and retrieving it for analysis with hand-held instruments. Salinity is currently being measured using the latter method, which could be improved as the water sample changes temperature and pressure as it is brought to the surface, which can affect the salinity

measurement.

1.3 Objectives

The objectives of this project are to design and develop a prototype device for measuring the salinity of the water beneath the ice shelf. The prototype should aid in investigating its feasibility and understanding the methodology for measuring salinity. It should set the foundation for a future device to be developed that can be used in the field. The final device should be able to withstand Antarctica's harsh temperatures and conditions, but these will only be secondary considerations in this project.

1.4 Scope & Limitations

This project's scope includes the design and development of a prototype device for measuring salinity. This includes researching the relevant literature that details devices with similar functionality, the theory behind measuring salinity, followed by the design and development of a prototype device that can test the properties of salt water and lead to a method of measuring salinity. The prototype development involves testing and evaluating the device to determine its effectiveness in measuring salinity. Additionally, this project should aim to develop the prototype as a separate probe and control unit. The scope does not extend to any development for the final device beyond the prototype nor the analysis of any data captured should the prototype be used in the field.

This project has a budget limitation of R2000 for the entire design, development and testing. This budget can only be spent through [UCT](#) with their approved suppliers and vendors. The project must be completed in 14 weeks from the start to the submission of the final report.

1.5 Report Outline

Following this introduction in Chapter 1, the literature review in Chapter 2 will give an overview of salinity, the methods of measuring it, and the devices used to measure it. The method of calculating salinity is cover in Chapter 3. This is followed by the design of the probe circuitry, its electrodes and a controller required to measure salinity and a controller in Chapter 4. Chapter 5 details the fabrication of the designed probe circuitry and the controller onto [Printed Circuit Boards \(PCBs\)](#), the correction made to them, and the waterproofing of the probe by casting it into epoxy. Chapter 6 details the evaluation of the probe's resistance measurement accuracy, following by an investigation into and evolution of a method to measure conductivity and to calculate salinity. Finally, Chapter 7 concludes the report with a summary of the project's objectives, the results obtained, and Chapter 8 provides recommendations for future work.

Chapter 2

Literature Review

2.1 Introduction

This literature review starts with introducing the concept of salinity and its history. It then discusses the importance and various uses of salinity measurements. The review then covers the various documented methods of measuring salinity, followed by a review of the devices that used conductivity to measure salinity, which is the industry standard. The review concludes with the theory and calculation of salinity from conductivity measurements.

2.2 Salinity Definitions

The most commonly understood definition of salinity relates to the total amount of dissolved *salts* in a solution. However, salinity's definition has had several more complex iterations over the last century. One of the first definitions of salinity was the total amount of dissolved *material* in grams in one kilogram of water [6], which is a dimensionless quantity that was expressed in [Parts Per Thousand \(%\)](#) or $g.kg^{-1}$ where most of the ocean water's salinity falls between 34.60% and 34.80% [6].

The problem with this definition lies in its testability. Trying to obtain the mass of the dissolved material through evaporation removed certain compounds, making this method inaccurate [7] and other methods of isolating the mass of the dissolved material had similar issues [6]. The need for testability led to salinity being redefined in 1969 to be related to the amount of chlorine present in the water, better known as chlorinity [6]. Chlorinity measurements were well established, and the salinity calculation from chlorinity was relatively simple, which is further discussed in [Section 2.3.1](#).

Around the same time as the salinity-chlorinity relationship was established, oceanographers began experimenting with using conductivity to measure salinity. Conductivity was more precise and straightforward than the titration required to measure chlorinity [8]. In 1978, the Practical Salinity Scale was established, which defined salinity in terms of conductivity and is regarded as the current definition of salinity [8]. While the conductivity measurement was considered easy, the salinity-conductivity relationship was more complex as it had to include corrections for temperature and depth as they both affect the conductivity of an electrolyte solution [9].

The Practical Salinity Scale uses dimensionless units of salinity, which are approximately equivalent to [Parts Per Thousand \(%\)](#) [10] in the current definition of salinity [11]. Although the Practical Salinity Scale is sometimes given in [Practical Salinity Units \(PSU\)](#), it is more technically correct to refer to

it as a certain Practical Salinity ‘on the Practical Salinity Scale PSS-78’ [8]. The salinity calculation from conductivity is further discussed in Section 3.1.

2.3 Salinity Measurement Methods

Salinity has had a long history of being measured using various methods with varying degrees of accuracy. Currently, the most common method of measuring salinity is using a [Conductivity, Temperature, Depth \(CTD\)](#) instrument. However, there are multiple alternative methods, most of which have been developed over the last three decades, a summary of which is provided in Table 2.1.

Table 2.1: Summary of the various methods of measuring salinity.

Method	Key Advantages	Key Disadvantages	Highest Accuracy
Chlorinity	<ul style="list-style-type: none"> Concisely defined Well established 	<ul style="list-style-type: none"> Requires titration Has human error 	0.01‰ [7]
Conductivity	<ul style="list-style-type: none"> Industry standard Automated devices available 	<ul style="list-style-type: none"> Complex relationship Requires temperature and depth corrections 	0.0002 PSU [12]
Density	<ul style="list-style-type: none"> Accounts for all dissolved material 	<ul style="list-style-type: none"> Complex relationship Requires temperature correction 	0.003 PSU [13]
Microwave Radiation	<ul style="list-style-type: none"> Measurable from a distance including from space 	<ul style="list-style-type: none"> Requires many corrections Expensive instrument 	0.1 PSU [14]
Refractive Index	<ul style="list-style-type: none"> Compact devices available 	<ul style="list-style-type: none"> Complex relationship Requires temperature and pressure corrections 	0.4‰ [15]
Interferometry	<ul style="list-style-type: none"> High accuracy reported 	<ul style="list-style-type: none"> Large, complex instrument Difficult to implement 	0.001 PSU [16]
Electromagnetic Induction	<ul style="list-style-type: none"> Non-destructive 	<ul style="list-style-type: none"> Not well researched Large, high power instrument 	-

2.3.1 Salinity from Chlorinity

The chemical composition of ocean water with a salinity of 35‰ contains 19.35‰ of Chlorine and 10.77‰ of Sodium with the following most common ions only accounting for just above 3‰ of the total dissolved solids in the water [17]. This allowed oceanographers to determine that the salinity of ocean water was directly proportional to the amount of chlorine in the water, which holds true provided the ratios of the dissolved materials in the water remained constant. The chlorinity of a solution has an established definition, which is ‘the mass of silver required to precipitate completely the halogens

in 0.328 523 4kg of the ocean-water sample' [18] which could be tested using titration. In 1969, an accurate relationship between these was established by Reference [18], shown in Equation 2.1, which was significantly more accurate than the evaporation method achieving accuracies within 0.01‰ [7] but was still limited by human error [8].

$$S(\%) = 1.80655 \times Cl(\%) \quad (2.1)$$

2.3.2 Salinity from Conductivity

The conductivity of a liquid is a measure its ability to conduct electrical current, which is related to the number of free electrons present in the liquid, which is in turn related to the number of ions present in the liquid [6]. In the case of salt water, the ions present are from the dissolved material, which salinity was previously defined on [6]. The relationship between salinity and conductivity accounts for all the ions in the water as opposed to just chlorine which is why it was considered a more apt measure of salinity [8]. Measuring conductivity was more accurate than titration, achieving accuracies within 0.0002 PSU [12]. The conductivity measurement is typically done using a CTD which measures the conductivity as well as the temperature and depth that are required to accurately calculate salinity. CTD devices are discussed further in Section 2.4 and the calculation of salinity from conductivity is further discussed in Section 3.1.

2.3.3 Salinity from Density

The density of pure water varies with temperature and is approximately 1000kg.m^{-3} at 4°C [19]. Adding denser materials to the water will intuitively increase its density. This concept is used to determine the quantity of added material using a density measurement, which can be used to calculate salinity [20]. The relationship between salinity and density is approximately linear as shown in Equation 2.2 where ρ is the density of the water, ρ_0 is the density of pure water, k is a proportionality constant, and S is the salinity of the water [21].

$$\rho = \rho_0(1 + kS) \quad (2.2)$$

The more accurate relationship is more complicated and includes a temperature correction defined by Reference [13]. While the accuracy of salinity from density was less than that from conductivity with accuracies within 0.003 PSU [13], Reference [22] still claimed that density was more appropriate to use as the standard potassium chloride solution used to calibrate the CTDs meters did not account for the variation of the ratios of conductive and non-conductive materials commonly present in salt water while the density of the water did.

2.3.4 Salinity from Microwave Radiation

The electromagnetic spectrum interacts uniquely with salt water, scattering, refracting, and reflecting when in contact with it or any material dissolved in it. Different temperature molecules in the water interact with electromagnetic waves differently, and the pressure of the water also varies this interaction. However, the most significant effect is from the presence of the dissolved material [23].

Microwave radiation is one section of the electromagnetic spectrum that takes advantage of this fact

to measure salinity [23]. Microwave radiation does not require direct contact with the water to make a measurement, making it possible to measure the salinity of a water sample from a far distance, including from space [24]. This necessitated the investigation of the relationship that could accurately predict salinity from a microwave reading [24]. The relationship required multiple different corrections as the microwave readings were found to be affected by **Sea Surface Temperature (SST)**, surface air pressure, surface air temperature, faraday rotation, and surface wind speed [14].

This research has allowed for the development of satellites that can measure the salinity, which has been used to develop global salinity maps as shown in Figure 2.1. The data measured using this method is reported to be accurate to within 0.1 **PSU** [14].

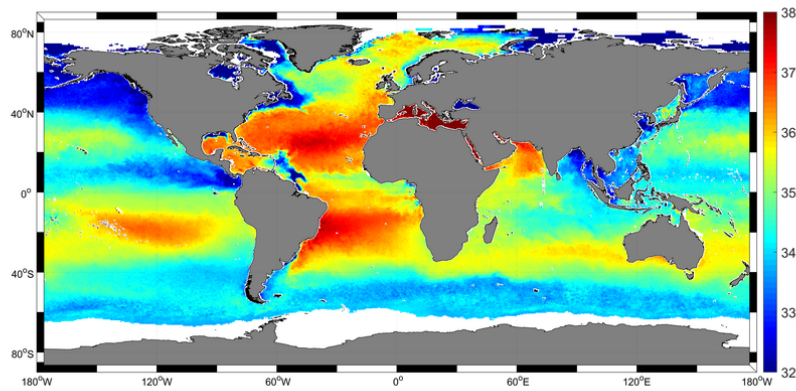


Figure 2.1: Global salinity map generated using satellite data [25].

2.3.5 Salinity from Refractive Index

The second measurement method that takes advantage of the electromagnetic spectrum interaction uses the visible light spectrum to measure the water's refractive index. The relationship between salinity and refractive index is similarly complex, requiring a 27-term equation that includes the effect of pressure and temperature. The refractive index equation is defined a range of $500 - 700\text{nm}$ in wave length, $0 - 30^\circ\text{C}$ in temperature, $0 - 40 \text{ PSU}$, and $0 - 11000\text{dbar}$ in pressure, and it holds an accuracy of $0.4 - 80 \text{ parts per million (ppm) PSU}$, decreasing with increasing pressure. [26]

Refractometers are used to measures the refractive index of water and as only a small amount of the sample is needed, these devices are relatively compact. Two notably compact versions have dimensions of $22.5\text{mm} \times 22.5\text{mm} \times 120\text{mm}$ [15] and $40\text{mm} \times 40\text{mm} \times 70\text{mm}$ [27] which have achieved accuracies of 2 and 83 $\%$ **PSU** respectively.

2.3.6 Salinity from Interferometry

The last measurement method that uses the electromagnetic spectrum is interferometry. Interferometry involves generating two identical light waves on the visible spectrum, passing one through the sample and the other through a non-interfering medium, and then comparing the two waves. The comparative

gain and phase shift between the two waves can be used to identify the salinity of a sample of salt water [28].

This method has varying implementations, each with varying results. Reference [16] reported to be accurate within 0.001 PSU using a Michelson interferometer and other researchers have reported other accuracies using different interferometers [29, 30, 31]. The refractometer has the disadvantage of being a large instrument requiring precisely aligned and spaced mirrors to direct the light waves, making it difficult to implement in a compact device.

2.3.7 Salinity from Magnetic Permeability

Similarly to conductivity, a liquid's magnetic permeability is related to the number of ions present in it. The more ions present in the liquid, the stronger the magnetic alignment that the liquid can generate, increasing its magnetic permeability. In salt water, this is related to the total dissolved solids [32].

Several methods are available for measuring a liquid's magnetic permeability, including [Inductance \(L\)](#), [Capacitance \(C\)](#), [Resistance \(R\)](#) ([LCR](#)) meters [33], resonant circuits [34], magnetic force sensors [35], and a permeability bridge [36]. These methods all have the advantage of not requiring direct contact with the salt water to make a measurement, which allows for the sample to remain undisturbed, unlike conductivity and other methods which may be destructive [37]. While the measurement of the magnetic permeability is well-defined, the relationship between it and salinity has yet to be thoroughly investigated. Additionally, the equipment required to measure the magnetic permeability is relatively large and typically has a high power consumption, making it difficult to compact for use in remote environments.

2.4 Salinity Measurement Devices using Conductivity

There are several commercial [CTD](#) devices available from small handheld devices such as the [Salinity Pen](#) to large oceanographic research devices such as [Ocean Exploration's CTD](#). These devices are used in various applications with varying prices and accuracies. The fundamental concept of the device involves placing two electrodes in a sample of water, applying a voltage across them, and measuring the water's response. This is paired with a temperature and depth correction, which allows a salinity value to be calculated, which is discussed in Section 3.1. Unfortunately, most of [CTD](#)'s technology is proprietary so the exact workings of their devices are not published.

Some researchers have developed their own [CTD](#) devices for specific applications. A study investigating the effect of human activities that alter the salt concentration of water sources such as lakes, ponds and wetlands in Illinois, USA, developed their own [CTD](#). The device reported an average error of 6% in the laboratory validation and 11% in the field validation. It used an alternative approximation of converting the conductivity to salinity, which used single voltage readings to measure the resistance of the water samples, which were then used to create a sensor-specific mathematical model to convert the resistance to salinity [38]. The voltage readings showed a non-linear relationship with between resistance and voltage, similar to that covered by Reference [39]. A similar device was shown on a forum with a similar design principle; however, this one was significantly less advanced, making no attempt to correlate the measured resistance values to a salinity value [40].

2.4. Salinity Measurement Devices using Conductivity

Researchers at Uppsala University in Sweden developed a nano CTD probe that measured $7.5 \times 3.5\text{mm}$ in size, shown in Figure 2.2. The probe contained everything required for an accurate salinity measurement, and each of the sensors achieved a high degree of accuracy. The probe achieved a high r^2 value of 0.9787 and a standard deviation of 2.37% using an alternating current at 42kHz to measure the conductivity. This design indicated that miniaturized salinometers are viable and could be used in devices such as bio-loggers on marine animals. [41]

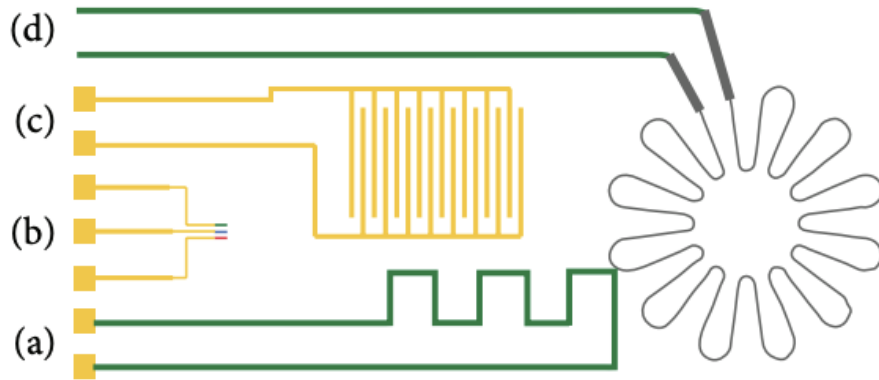


Figure 2.2: The schematic of a CTD probe developed by researchers at Uppsala University in Sweden which design contains (a) a temperature sensor, (b) three relatively small electrodes for pH and Cl⁻ concentration, (c) conductivity electrodes, and (d) a strain gauge for the pressure membrane sensor.

The design is $7.5 \times 3.5\text{mm}$ in size [41].

Chapter 3

Theory Development

3.1 The Calculation of Salinity From Conductivity

Salinity meters that use electrical conductivity are commonly known as [CTDs](#). As depth is a measurement derived from pressure, CTp is the preferred designation when performing calculations [8], which allows for the conductivity of a sample of water to be denoted by $C(S, T, p)$ where conductivity is a function of salinity S , temperature T , and pressure p which is the convention in oceanography [8]. Pressure in the salinity equation is taken relative to sea level where $p = 0\text{dbar}$ is equivalent to an absolute pressure of $P = 101\,325\text{Pa}$ [11]. Using decibars (dbar) for pressure is a common practice in oceanography as it is a unit of pressure roughly equivalent to one meter of water depth [42].

The Practical Salinity Scale defines Practical salinity S_p in terms of a conductivity ratio K_{15} , which is the conductivity of a sample of water at a temperature of 15°C and a pressure equal to one standard atmosphere divided by the conductivity of a standard potassium chloride solution at the same temperature and pressure. The standard potassium chloride solution is 32.4356g of KCl dissolved in 1.000kg of water, and when the ratio between the conductivity of a sample of water and the standard solution, or K_{15} , equals 1, the Practical Salinity S_p is, by definition, 35. [11]

When K_{15} is not equal to 1, the Practical Salinity S_p can be calculated using the PSS-78 equation shown in Equation 3.1.

$$S_p = \sum_{i=0}^5 a_i (K_{15})^{i/2} \quad \text{where} \quad K_{15} = \frac{C(S_p, 15^\circ\text{C}, 0)}{C(35, 15^\circ\text{C}, 0)} \quad (3.1)$$

All the coefficients for the salinity-conductivity equations, including a_i , are given in Table 3.1.

To calculate the salinity of a sample of water that is not at 15°C and 0dbar , the conductivity ratio of the sample can be expanded into the product of three ratios, which are labelled R_p , R_t , and r_t respectively. The conductivity measurement taken in the field $C(S_p, t, p)$ is related to the conductivity of the standard solution $C(35, 15^\circ\text{C}, 0)$ which the device is calibrated with and is represented by R in Equation 3.2. [11]

$$R = \frac{C(S_p, t, p)}{C(35, 15^\circ\text{C}, 0)} = \frac{C(S_p, t, p)}{C(S_p, t, 0)} \cdot \frac{C(S_p, t, 0)}{C(35, t, 0)} \cdot \frac{C(35, t, 0)}{C(35, 15^\circ\text{C}, 0)} = R_p R_t r_t \quad (3.2)$$

check In order to calculate the salinity of the sample, R_t must be found, which takes a similar form to

3.1. The Calculation of Salinity From Conductivity

K_{15} . r_t is first calculated using the temperature of the sample

$$r_t = \sum_{i=0}^4 c_i t^i \quad (3.3)$$

following which R_p is calculated using the sample's pressure p , temperature t and conductivity ratio R ,

$$R_p = 1 + \frac{\sum_{i=1}^3 e_i p^i}{1 + d_1 t + d_2 t^2 + R [d_3 + d_4 t]} \quad (3.4)$$

and finally R_t is calculated using r_t , R_p and R .

$$R_t = \frac{R}{R_p r_t} \quad (3.5)$$

For a sample temperature of $15^\circ C$ and pressure of 0dbar , r_t and R_t both equal 1, which leaves R_t equal to R and thus Equation 3.1 can be used to calculate the Practical Salinity S_p . For temperatures other than $15^\circ C$, the Practical Salinity S_p can be calculated using Equation 3.6 where $k = 0.0162$. [11]

$$S_p = \sum_{i=0}^5 a_i (R_t)^{i/2} + \frac{t - 15}{1 + k(t - 15)} \sum_{i=0}^5 b_i (R_t)^{i/2} \quad (3.6)$$

Table 3.1: Coefficients for the PSS-78 equations [11].

i	a_i	b_i	c_i	d_i	e_i
0	0.0080	0.0005	$6.766097 \cdot 10^{-1}$		
1	-0.1692	-0.0056	$2.00564 \cdot 10^{-2}$	$3.426 \cdot 10^{-2}$	$2.070 \cdot 10^{-5}$
2	25.3851	-0.0066	$1.104259 \cdot 10^{-4}$	$4.464 \cdot 10^{-4}$	$-6.370 \cdot 10^{-10}$
3	14.0941	-0.0375	$-6.9698 \cdot 10^{-7}$	$-4.215 \cdot 10^{-3}$	$3.989 \cdot 10^{-15}$
4	-7.0261	0.0636	$1.0031 \cdot 10^{-9}$	$-3.107 \cdot 10^{-3}$	
5	2.7081	-0.0144			

Note that the coefficients a_i precisely sum to 35 such that the Practical Salinity S_p is 35 when K_{15} or $R_t = 1$ as per Equation 3.1 and Equation 3.6. Additionally, the coefficients b_i precisely sum to 0 such that the Practical Salinity S_p does not depend on the temperature of the water when $R_t = 1$ as per Equation 3.6. [11]

Equation 3.1 to Equation 3.6 are valid for $2 < S_p < 42$ and $-2^\circ C < t < 35^\circ C$ and $0\text{dbar} < p < 10\,000\text{dbar}$ [11]. The range for salinity has been extended using estimations by Reference [43] for $0 < S_p < 2$ and Reference [44] for $42 < S_p < 50$.

The temperatures used in Equation 3.1 to Equation 3.6 are on the IPTS-68 scale [45] and have not been corrected to the currently used ITS-90 scale [46]. In order to correctly calculate the salinity, the

temperatures should be converted to the IPTS-68 scale using the equation $t_{68} = 1.00024t_{90}$ before calculating salinity [46].

3.2 Current Fringing in Conductive Materials

Current fringing or current spreading, not to be confused with magnetic fringing, occurs when an electrical current flowing through a conductive material spreads like a magnetic field. This is a phenomenon that is particularly prevalent and well studied in the manufacturing of [Light Emitting Diodes \(LEDs\)](#) where the current spreading can be a significant factor in the efficiency of the device [47, 48, 49].

The effect of current spreading in typical conductors is mostly negligible; if the material's conductivity is high enough and its cross-sectional area is small, the current spreading is minimal. However, if a conductor has a significantly larger cross-sectional area than the current requires, such as electrodes in salt water, the current spreading can become a significant factor in its conductivity. This version of current spreading has been studied and is documented for conductors of constant conductivity. [50]

Chapter 4

Design

4.1 Salinity Measurement Method

The industry standard for measuring conductivity is the [CTD](#), which calculates salinity using conductivity, temperature and depth measurement. Section [2.3](#) discussed several alternative methods of measuring salinity. The temperatures, environment and remote nature of the Antarctic make most of these methods difficult or impossible to use. Additionally, the final device was required to fit through an ice core hole of 110mm in diameter. While the prototype does not need to directly meet this requirement, it must be designed such that a future iteration can.

Refractometers and chlorinity titrations have the same drawbacks as the currently used hand-held [CTD](#), where capturing a water sample and bringing it to the surface alters its temperature and pressure, which may alter its salinity measurement. Microwave radiation has a lower-than-desirable accuracy. In addition, the instruments that measure it, as well as densitometers and interferometers, are expensive and complex beyond the author's expertise. Electromagnetic induction is one of the more promising methods because it is a nondestructive method of measuring salinity, which allows samples to be used for alternative measurements afterwards. However, as mentioned in Section [2.3.7](#), the electromagnetic and salinity relationship has yet to be thoroughly researched, and it requires a high power consumption. This latter is a significant issue in Antarctica as storing power is challenging at very low temperatures, not to mention transporting the device.

The conductivity, temperature and depth method was determined to be the most viable for this project as it is the industry standard, and the author has significant experience with [PCB](#) design and electronics. Additionally, it has been proven that it can be miniaturized, as mentioned in Section [2.4](#), making it the most likely method to fit through the ice core. This and the other methods face a challenge because the Practical Salinity Scale is not defined for sub-zero temperatures, which may be a problem in Antarctica and should be researched further.

4.2 Conductivity Electrode Material

Ideal electrodes for measuring conductivity in salt water have zero resistance and infinite corrosion resistance and can confine the electrical current in the water to a specific known volume. Electrodes with zero resistance would allow the resistance measured using the electrodes to be entirely due to the water. However, most conductive materials have a conductivity in the order of $10^8 Sm^{-1}$, which causes negligible resistance compared to salt water which has a conductivity range of $0 - 5Sm^{-1}$ [51].

The infinite corrosion resistance will allow the electrodes to last indefinitely in the highly corrosive saltwater environment, and several materials with near-perfect corrosion resistance are used in marine environments, which will be able to satisfy this criterion. The confinement of the electrical current allows for an easier calculation of the conductivity ρ from resistance R if the cross-sectional area A and length l of the water between the electrodes is known as shown by Equation 4.1.

$$\rho = \frac{RA}{l} \quad (4.1)$$

Several materials known for their corrosion resistance include non-precious metals such as aluminium, stainless steel, nickel and copper alloys, and titanium, as well as precious metals such as gold, silver, and platinum. Precious metals are known for having a significantly higher corrosion resistance. However, they are also significantly more expensive.

Choosing the electrode's material involved prioritising high corrosion resistance and low resistance while being restricted to materials that were attainable and within this project's budget. Titanium is the most corrosive resistant of the non-precious metals and has an acceptable conductivity of $2,3 \cdot 10^6$ which is about 25 less than that of copper [52]. Titanium wire was available through off-cuts from a project being conducted by the Chemical Engineering Department of the University of Cape Town. Thus, it was possible to use this material for the electrodes.

Of the precious metals, gold is one of the most accessible as it is a common material used in PCBs manufacturing primarily because of its high corrosion resistance paired with a high conductivity of $49 \cdot 10^6$ which is similar to copper's conductivity [52]. Electroless Nickel Immersion Gold (ENIG) PCB manufacturing is a process where nickel, followed by gold, is deposited onto the copper of the PCB using chemical reactions. While this process is expensive compared to standard PCB manufacturing, it is affordable within this project's budget and made gold a possible electrode material.

Both gold and titanium were used for this project, as they could be manufactured into electrodes of different shapes, which allowed for comparative testing of the materials and the shapes. The electrode design is further discussed in Section 4.3.

4.3 Conductivity Electrode Design

Gold electrodes made using the ENIG PCB manufacturing process were chosen as the device's primary electrodes. The PCB manufacturing process allowed the electrodes to be made with a known area and length of the water between the electrodes, allowing for a more accurate conductivity calculation.

Salt water does not have a constant resistivity with respect to voltage [38],[53]. In order to isolate the non-linear resistance-voltage curve, the resistance of the water between the electrodes needed to be measured at different voltages while other factors were kept constant. This necessitated close attention to the fringing effect of the electrical current between the electrodes. Wide, flat pads were used on the PCB electrodes, which were placed close together to reduce the current spreading. Additionally, a fringe guard was added to the electrodes, which consisted of a pad that outlined the main conductivity pads that repeated the same voltage as the main pads using an op-amp with unity gain. Ideally, the fringe guard would saturate the volume around the main pads with current and thus prevent them

from fringing. PCB connectors to attach the electrodes to a probe were added to this configuration, as shown in Figure 4.1.

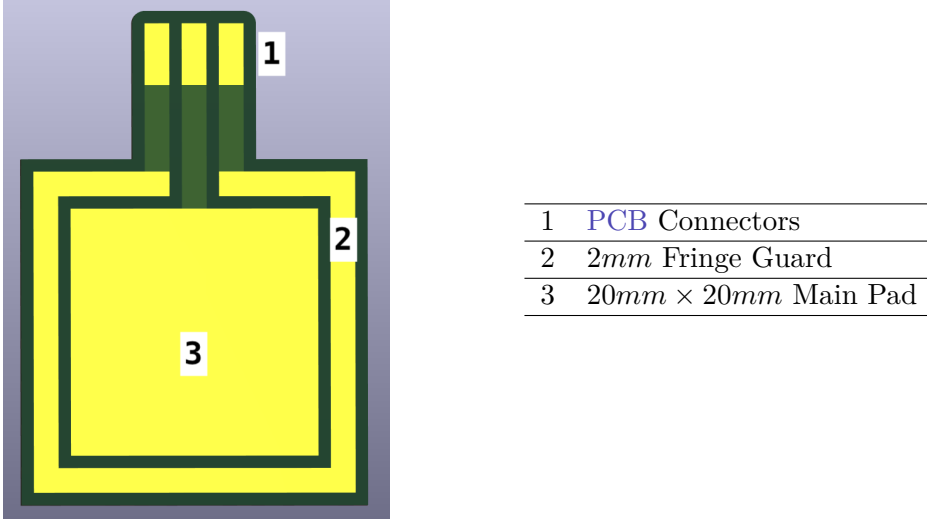


Figure 4.1: The gold electrode PCB design.

The dimensions of the gold electrodes were chosen to be round values, with the pads having a large surface area and being placed relatively close together. However, they could not be placed too close together as this could prevent water from effectively flowing between them. Theoretically, this would reduce the proportion of fringing versus linear current between the electrodes. This theory is based on the electrical field fringing effect found in capacitors: take two capacitor pads that are placed close together, which experience a certain amount of fringing; if the area of those two pads increases, the quantity of fringing field will increase relative to the side length while the quantity of linear field which would increase relative to the square of the side length [54, 55].

The second method employed to reduce the fringing effect was to keep the resistance between the pads low, which lowers the voltage required to generate a current through the water, which would theoretically further reduce the current fringing. This theory is also based on capacitors where higher voltages generate stronger electrical fields that spread, or fringe, more.

The gold electrodes were designed with a $20\text{mm} \times 20\text{mm}$ main pad with a 2mm wide fringe guard surrounding it and a spacing between the electrodes of 10mm . The expected resistance was then calculated to be between $3,75\Omega$ and $6,25\Omega$ using Equation 4.1 and conductivity values for salinities between 40 and 25 PSU [11].

The titanium electrodes were less complicated to design as they only had two variable parameters: their length and spacing. However, as they were made from titanium wire, the fringing effect between them could not be reduced using the same method as the gold electrodes. Thus, it was decided to use the gold electrode to evaluate an accurate method for determining conductivity, which could then be applied to the titanium electrodes, where the fringing effect could be mathematically corrected.

The titanium electrodes are significantly more cost-effective than the gold electrodes. Thus, if an accurate method for determining salinity using them is developed, they will likely become the primary electrodes of the final device. The titanium wire available for this project was 1mm in diameter and to

account for the unknown resistance between the electrodes, the design allowed for adjustable spacing between the electrodes and adjustable electrode length.

4.4 Resistance Measurement Method

The most common and practical method of measuring resistance is using a resistor divider circuit, which this project chose to employ. While current measuring [Integrated Circuits \(ICs\)](#) exist, the low current ($< 1A$) versions use the same resistor divider principle. Thus, it was considered to be more cost-effective and configurable to design the resistor divider circuit.

The electrodes were chosen to be the R_2 resistor in the voltage divider, and the R_1 resistor was chosen to be a significantly larger, known resistance. The large R_1 value allowed a full range of voltages to be applied to the resistor divider while keeping the voltage across the electrodes low, which was advantageous for the reasons mentioned in Section 4.3. This configuration also prevented the circuit from being short-circuited if the electrodes were to touch, as the R_1 resistor would limit the current. The voltage drop across the electrodes was then amplified using an op-amp to increase the resolution of the voltage measurement.

4.5 Circuit Overview

The resistor divider circuit was designed to be printed onto a [PCB](#) (herewith referred to as the probe) manufactured with JLCPCB. [PCB](#) manufacturing is cost-effective, has a high precision relative to hand soldering, and the process was familiar to the author, making it the ideal method for creating the prototype. However, the resistor divider circuit required a few additions to increase its versatility and testing capability, an overview of which is shown in Figure 4.2.

The voltage driving the resistor divider was provided by a [Digital to Analogue Converter \(DAC\)](#) so that the voltage could be varied and salt water's voltage-resistance relationship could be determined. The [DAC](#) model was chosen from the [DACs](#) available on the JLCPCB's website. The model DAC53401 was ultimately chosen for its high updated time of $10\mu s$ and its advanced functionality, which allowed it to output square, triangle, and sawtooth waves. This functionality could be used to perform high-frequency tests in addition to linear voltage sweeps.

A typical configuration of a [DAC](#) is to connect its output to the non-inverting input of an op-amp, which would be connected to the base of a transistor. The transistor's emitter would then be connected to the inverting input of the op-amp. This configuration allows a higher current to be drawn than the [DAC](#) can provide while maintaining the specified output voltage. The DAC53401 has an internal op-amp and a feedback input, which allows a transistor to be connected as shown in Figure 4.2 to achieve the same outcome.

Sets of switches added to the circuit allowed the voltage produced by the [DAC](#) to be directed to an R_1 resistor, then across to a pair of electrodes or to a calibration resistor. The switch model TS3A4751 was chosen from JLCPCB, which contained four switches in its [IC](#), as it was very cost-effective for its low and consistent on-state resistance of around 0.7Ω . The circuit required three switching points: one for choosing the R_1 resistor, one for choosing the anode and one for choosing the cathode.

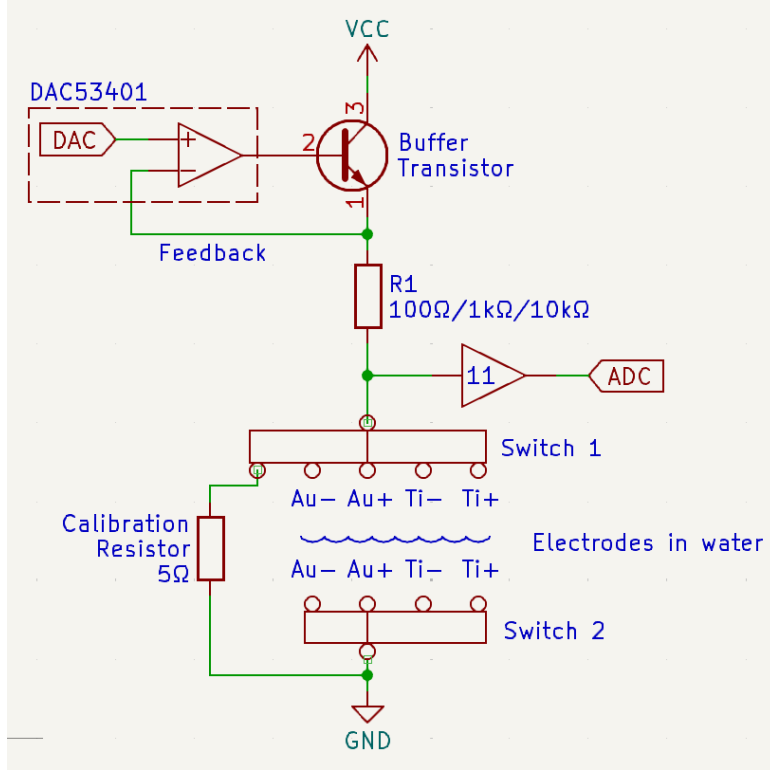


Figure 4.2: A simplified representation of the resistance measuring circuit.

It was decided to give the R_1 resistor alternate resistances to allow for any possible resistance between the titanium electrodes or unforeseen errors. The R_1 value chosen to pair with the gold electrodes was 100Ω as it was the smallest e12 series resistance that would prevent the board from drawing too much current and burning out the traces or switches. The final resistances were chosen to be 100Ω , $1k\Omega$ and $10k\Omega$, which would be used when the resistance between the probes was $1\Omega - 10\Omega$, $10\Omega - 100\Omega$ and $100\Omega - 1k\Omega$ respectively. This configuration allowed for a minimum resolution of 11% of V_{DAC} for the voltage measurement by the [Analogue to Digital Converter \(ADC\)](#) as shown by Equation 4.2.

$$\frac{1\Omega}{1\Omega + 100\Omega} * V_{DAC} * 11 = 11\%V_{DAC} \quad (4.2)$$

$$\frac{10\Omega}{10\Omega + 100\Omega} * V_{DAC} * 11 = 100\%V_{DAC} \quad (4.3)$$

The anode switch, denoted as switch 1 in Figure 4.2, allowed R_1 to be connected to any of the four electrodes or to the calibration resistor of 5Ω , and the cathode switch, denoted as switch 2 in Figure 4.2, allowed any electrode to be connected to ground. An example of measuring the resistance between the titanium electrodes would be to connect switch 1 to Ti+ and switch 2 to Ti, allowing the voltage drop to be measured. This configuration also allows current to flow in both directions between electrodes, which can prevent an excessive buildup of chlorine gas or sodium electroplating on the electrodes or electrolysis of the water by taking a resistance measurement in both directions in rapid succession.

To increase the accuracy of the R_1 resistors, they were made by placing multiple high-accuracy resistors in parallel, which decreases their resistance uncertainty. The total uncertainty of the parallel resistance $\delta_{R_{total}}$ is decreased by a factor equal to number of parallel resistors n compared to each resistance's

uncertainty δ_R as shown by Equation 4.4 to Equation 4.6.

$$R_{total} = \left[\sum_{i=1}^n \frac{1}{R_i} \right]^{-1} = \left(\frac{n}{R} \right)^{-1} = \frac{1}{n} \cdot R \quad (4.4)$$

for a function $f(x_1, x_2, \dots, x_n)$, its tolerance $\delta_f = \sqrt{\sum_{i=1}^n \left(\frac{\partial f}{\partial x_i} \delta x_i \right)^2}$ (4.5)

$$\therefore \delta_{R_{total}} = \sqrt{\left(\frac{\partial R_{total}}{\partial R} \delta R \right)^2} = \sqrt{\left(\frac{1}{n} \delta R \right)^2} = \frac{1}{n} \delta_R \quad (4.6)$$

The R_1 resistors were made from 3 parallel resistors, each with tolerance $\pm 1\%$ giving a total tolerance of $\pm 0.3\%$ and the calibration resistor was made from 4 parallel resistors with tolerance $\pm 1\%$ giving a total tolerance of $\pm 0.25\%$.

A last switch point was added to the circuit for the gold electrode's fringe guards, an example of which is shown in Figure 4.3. The voltage from R_1 was routed to a buffer op-amp with unity gain. Its output was then connected to the fringe guard, which effectively repeated the same voltage as the main pad while not affecting any measurements using them. The other fringe guard could be switched to ground, allowing a current to be generated between the two. This current would ideally absorb any possible fringing from the main pads. The same switch point also allowed the fringe guards to be electrically disconnected to test their effectiveness and to determine if they interfered with the measurement. Lastly, as the fringe guards held the same voltage difference as the main pads and, in theory, had a higher resistance due to their smaller area, the current flowing between them was assumed to be less than that of the main pads; thus, there was no need to limit the current from the op-amp.

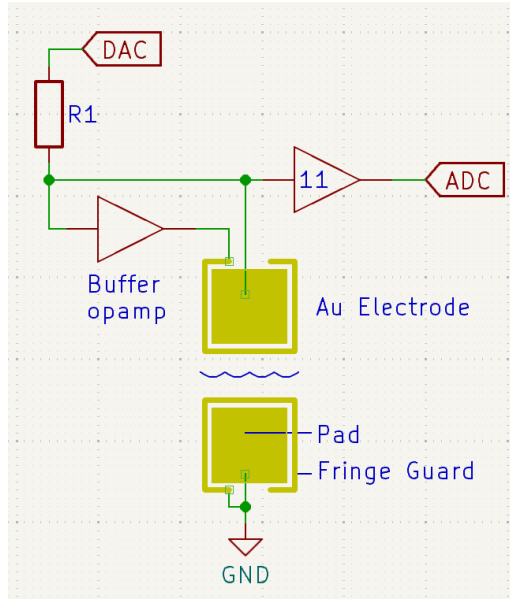


Figure 4.3: A simplified representation of the resistance measurement circuit using the gold electrodes with the fringe guard.

4.6 Salinity Calculation and Display

In order to measure the salinity of the water, the probe [PCB](#) would be lowered through the ice core hole into the water to capture salinity readings at various depths. The measurements could either be captured automatically at preprogrammed depth or time intervals or triggered by the user using a controller. The latter method was chosen for this project because it is a more user-friendly approach, allowing researchers to control precisely which depths the salinity measurements are made and giving them live updates about the probe's status and onboard sensors.

The controller was a straightforward [PCB](#) with input buttons and rotary switches, two 7-segment displays, a [Recommended Standard #485 \(RS-485\)](#) communication port and a simple microcontroller.

Saltwater has a high [Electromagnetic Interference \(EMI\)](#), which interferes with all wireless communication [56]. While high-power wireless communication is viable for ranges up to 70m, it is more reliable, cost-effective, and power efficient to use a wired connection [57]. [RS-485](#) is a robust, long-range embedded communication protocol that only requires a simple [IC](#) to use, making it ideal for this project. Additionally, the author was familiar with this protocol and had previous board-to-board communication experience with it.

[Universal Asynchronous Receiver-Transmitter \(UART\)](#) to [RS-485](#) converters are common as most microcontrollers have a [UART](#) communication port. This project used half-duplex [RS-485](#) as it is the industry standard, and it is more cost-effective than full-duplex [RS-485](#), which requires an additional [UART](#) to [RS-485](#).

The microcontroller was chosen from the STM32F030 series as it did not need to perform any complex calculations, and the author was familiar with this series.

With an external controller, a waterproofed probe could be lowered into the water to measure its salinity. The chosen method of waterproofing the probe was to coat it with epoxy resin, as this was the most familiar and cost-efficient method available. The other notable option is to create a waterproof housing for the probe, but this can be complex and expensive. In addition to the circuitry shown in Figure 4.2, the probe had a temperature and depth sensor, which are discussed in Section 4.7, an [RS-485](#) communication port and a microcontroller. The microcontroller was chosen from the STM32F4 series as it is the most cost-effective series with a [Floating Point Unit \(FPU\)](#), allowing the salinity to be calculated on board as per the equations in Section 3.1.

4.7 Temperature and Depth Measurement

Waterproof depth sensors were too expensive for this project's budget, costing around \$100. An alternative approach is to use a non-waterproof pressure sensor that is isolated from the water using a flexible membrane that allows the external pressure to be transmitted to the sensor. The WF183DE pressure sensor was chosen as it was the most cost-effective sensor rated for above 50 meters of water pressure available at [JLCPCB](#). Should this approach fail, the backup plan was to use the controller to manually input a depth so that the salinity could still be calculated.

The temperature sensor was an arbitrarily chosen surface-mount sensor with high accuracy of $\pm 0.3^{\circ}\text{C}$

4.7. Temperature and Depth Measurement

and a wide temperature range of -45 to 130°C . Epoxy resin is a poor thermal conductor [58]. Thus, the temperature sensor should be coated with a very thin layer of epoxy when the probe PCB is cast, allowing for a more accurate measurement. The choice of microcontroller and pressure sensor also provided this board with two alternative temperature sensors, which were less accurate but could be used in the event that the primary temperature sensor failed.

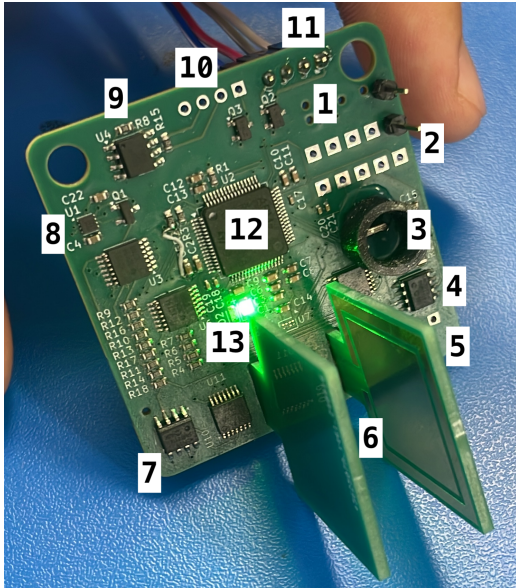
Chapter 5

PCB Construction, Adjustments and Code

5.1 PCB Design

The probe, controller and gold electrodes were fabricated on [PCBs](#), which were designed using KiCad software and manufactured with JLCPCB. The KiCad design files can be found in the Git repository linked in Appendix C. The gold electrodes were trivial, only requiring a single layer [PCB](#) with simple pads and traces.

The probe [PCB](#) was the most complex. It was fabricated on a 4-layer [PCB](#) with dimensions of $50 \times 50\text{mm}$, shown in Figure 5.1. JLCPCB offered a discount for 4-layer [PCBs](#) that were smaller than $50 \times 50\text{mm}$ in size. While the probe should ideally be as small as possible to fit through the ice core, it was not designed to be smaller than $50 \times 50\text{mm}$ to allow for a more straightforward debugging process.



1	Programmer Port
2	Test Points
3	Pressure Sensor in a Protective Housing
4	11× Gain Op-Amp
5	Titanium Electrode Port
6	Gold Electrodes
7	Unity Gain Buffer Op-amp
8	DAC and Buffer Transistor
9	UART to RS-485 Converter
10	RS-485 Port
11	UART Port
12	STM32F4 Microcontroller
13	LEDs

Figure 5.1: The probe PCB with the gold electrodes attached and some adjustments made

Note 1: The rest of the titanium electrode ports are behind the gold electrode.

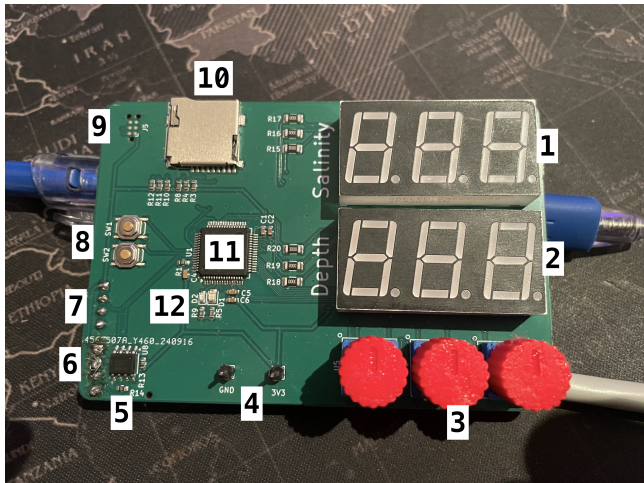
Note 2: The other ICs present are the TS3A4751 switches.

The probe was designed with the resistance measuring circuitry, the temperature and pressure sensors, the microcontroller, the [UART](#) to [RS-485](#) converter and the [RS-485](#) port mentioned in Chapter 4.

The gold and titanium electrode ports, which were placed at the bottom of the probe, were designed to allow them to be soldered perpendicular to it. The other methods of attachment all presented a fundamental disadvantage: connecting them with wires added extra resistance, and attaching them parallel to the board or perpendicular facing downwards was considered too complex.

Several adjustments were made to facilitate easier debugging. A [UART](#) port was added next to the [RS-485](#) port to allow for data to be streamed to a computer using a [UART](#) to [Universal Serial Bus \(USB\)](#) converter. Both ports also had reverse polarity protection added to prevent unintentional board damage. [LEDs](#) were added next to the microcontroller, and a programmer port and test points were added at the top of the board to allow for visual feedback and circuit analysis. With the programmer and communication ports at the top of the board and the electrodes at the bottom, the probe could safely be submerged while transferring its data to a laptop.

The controller [PCB](#) was fabricated on a 2-layer board, which is shown in Figure 5.2, as the components were too large to fit on a $50 \times 50\text{mm}$ 4-layer board. JLCPCB offered a similar discount for 2-layer [PCBs](#) that were less than $100 \times 100\text{mm}$ in area. Ultimately, the controller dimensions were $100 \times 60\text{mm}$, which could comfortably fit all the components while taking advantage of JLCPCB's discount.



1	Salinity 7-Segment Display
2	Depth 7-Segment Display
3	Rotary Switches
4	Power Input
5	UART to RS-485 Converter
6	RS-485 Port
7	UART Port
8	Input Buttons
9	Programmer Port
10	SD Card Port
11	STM32F0 Microcontroller
12	LEDs

Figure 5.2: The controller PCB with the rotary switch caps attached

The controller was designed with the buttons, the rotary switches, the 7-segment displays, the [UART](#) to [RS-485](#) converter, and the [RS-485](#) port mentioned in Chapter 4. The 7-segment displays were designated to display the salinity and depth of the water by default using silkscreen text, but they could be changed to display anything using software. The components were placed user-friendly, allowing for easy use of the buttons and rotary switches. Similarly to the probe, [LEDs](#), a [UART](#) port and a programmer port were added to the board to allow for debugging of the board. It should be noted that an SD Card Port was added for future development and testing but was not utilised during this project.

5.2 PCB Adjustments

Three adjustments were made to the probe [PCB](#) to ensure it functioned as required, excluding the soldering of headers and the gold electrodes. Firstly, one of the microcontroller's pins was unconnected

to power and was corrected by soldering a wire between it and a pin with power, which can be seen on the left of the microcontroller. Secondly, the footprint of the pressure sensor was horizontally reversed, which was corrected by flipping and soldering the depth sensor vertically. A protective case was added around the pressure sensor to prevent it from being damaged during testing. The casing would later function as the support for the waterproof membrane mentioned in Section 4.7.

Lastly, both op-amps were incorrectly chosen as they required a rail-to-rail voltage of 6V to operate, higher than the 3.3V provided. Thus, they were replaced with an alternative op-amp model with the same footprint. The temperature sensor also had an incorrect footprint, but this could not be rectified as it was discovered after the board was fabricated. Thus, the temperature sensor was not soldered to the board. The pressure sensor's onboard temperature sensor was used instead.

The controller PCB required no soldering adjustments. There was a minor error in the pin assignments of the rotary switches, but this was corrected in the software and did not require any hardware changes. Switch caps were 3D printed and attached to rotary switch shafts to make them easier to turn, making the controller more user-friendly.

5.3 Probe Code

The significant steps in measuring salinity are measuring the water's conductivity, temperature and pressure and then calculating its salinity. An overview of this process is shown in Figure 5.3.

The conductivity measurement was aimed at repeating the methodology that Reference [38] employed. This requires a voltage sweep of the water sample, which is then mapped to a conductivity. This devices specific mapping will have to be determined experimentally, as it is unique for different electrode sizes and materials. The voltage sweep is achieved by incrementing the output of the DAC from a given start to end voltage. At each step, the output of the DAC and the voltage drop across the calibration resistor and the electrodes are recorded.

To determine the resistance measuring accuracy, the resistance across the electrodes R_E was calculated using the voltage drop across the electrodes and across the calibration resistor R_C , as shown in Equation 5.1 to Equation 5.3. The electrode resistances R_E was calculated for each voltage sample and then averaged.

$$V_{ratio} = \frac{V_{DAC}A_{11}A_{ADC}\frac{R_E}{R_1 + R_E}}{V_{DAC}A_{11}A_{ADC}\frac{R_C}{R_1 + R_C}} = \frac{\frac{R_E}{R_1 + R_E}}{\frac{R_C}{R_1 + R_C}} \quad (5.1)$$

$$\frac{R_E}{R_1 + R_E} = V_{ratio} \frac{R_C}{R_1 + R_C} \rightarrow k \quad (5.2)$$

$$R_E = \frac{kR_1}{1 - k} \quad (5.3)$$

This method of calculating resistance using a voltage ratio with a known resistance allows the probe to nullify all scalar inaccuracies in the circuit, including the DAC, ADC and op-amp gain error, as

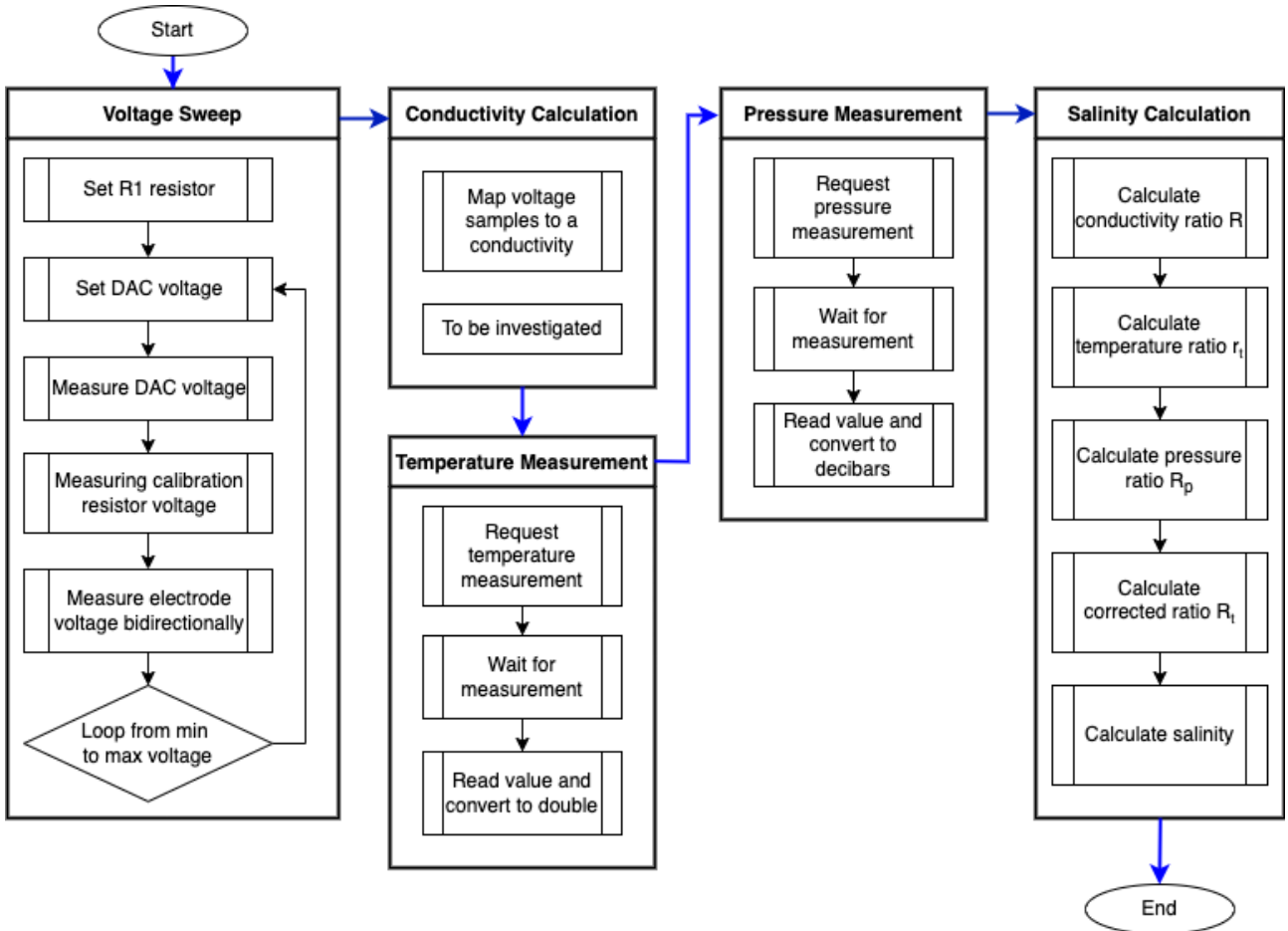


Figure 5.3: The flowchart for the probe code that measures salinity.

they will be present in both voltage measurements. However, this method is still vulnerable to offset inaccuracies, including **DAC** and **ADC** offset errors, op-amp input offset and input bias currents, the R_1 resistance errors and the resistance added by the switches and traces.

As previously mentioned, the pressure and temperature measurements are taken from the WF183DE pressure sensor. This sensor operates similarly for both measurements: a request is made to make a measurement, it can then be polled until the measurement is ready, and then the measurement can be read.

Once the conductivity, temperature and pressure measurements are taken and converted into the required units of Sm^{-1} , $^{\circ}C$ and $dbar$ respectively, salinity can be calculated as shown in Section 3.1. Additionally, if requested, any of the temperature, depth, resistance, or conductivity measurements can be calculated individually and transmitted to the controller.

5.4 Controller Code

The controller's primary function for the prospective user was to instruct the probe to take a measurement and display it. However, the controller was given additional functionality for testing and investigation purposes, which allowed the controller to update the probe's configuration.

The common-cathode 7-segment displays displayed the various measurements from the probe. The displays' digits were individually written to by writing the digit code and keeping the corresponding

digit's cathode low while keeping the others high. A timer controlled [Direct Memory Access \(DMA\)](#) was used to write to each digit in quick succession, giving the illusion of all the digits being on simultaneously.

The leftmost rotary switch was used to navigate the menu, which consisted of the default showing both salinity and depth, individual measurements of temperature, depth, resistance, conductivity, and salinity, and the probe's configurable parameters. The menu names were displayed on the top 7-segment display, and the selected menu item was displayed on the other. This created some limitations on what could be displayed. For instance, the best display of the word 'temperature' was 'teP', but all menu items had a unique, relatively clear name.

When the user selected a measurement menu item, the top switch was configured to request that measurement from the probe and display it; when the user selected a configuration menu item, the top switch was configured to update the probe's configuration. The other two rotary switches adjusted the probe's configurable parameters, further discussed in Section 5.5. The bottom switch was configured to reset the probe and the controller should an error occur.

5.5 Board-to-Board Communication

The probe and controller communicate using half-duplex [RS-485](#), which is converted on both sides to [UART](#). This makes the protocol effectively half-duplex [UART](#) communication from the perspective of the microcontrollers. The probe was configured to be in receive mode, where it would perpetually wait for a one-byte command from the controller. All the possible commands and expected transactions are shown in Figure 5.4.

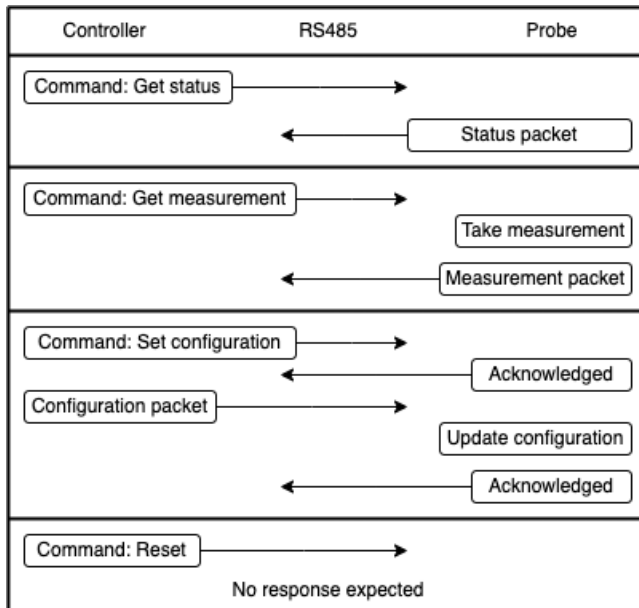


Figure 5.4: The flowchart for the board-to-board communication protocol denoting the four transaction types. The arrows denote the direction of the packets being sent over the [RS-485](#) link.

While not directly available to the user, the controller could request a status byte to which the probe would respond with *idle*, *busy* or *error* depending on its state. This allowed for some simple error

checking and communication flow, which could be integrated into more robust error handling in the future. When the user requests a measurement, the controller sends the corresponding request command, to which the probe will respond with the measurement data. The data was returned as a 3-byte, fixed-point float.

When the user requested a configuration update, the controller transferred a configuration packet using the expected transaction. Once the probe was entirely cast in epoxy resin, the configuration could only be updated this way, so all possibly useful, configurable parameters are included. This included which electrode to use (including whether to use the fringe shield), the R_1 resistor to use, the directionality of the resistance measurement (unidirectional or bidirectional), the voltage sweep start, end and number of steps, among other parameters. Some parameters, such as the directionality, were unlikely to be changed from their default value (bidirectional) but were included to cover any unforeseen circumstances.

When the user resets the boards using the controller's bottom switch, a reset command was sent to the probe before the controller reset itself. This command allows for resetting the probe should a system error occur. However, this only works provided the [RS-485](#) link is still operational. Otherwise, the entire system must be powered off and on again to reset the probe. The reset on both microcontrollers is triggered using software to set the [System Reset Request \(SYSRESETREQ\)](#) bit in the [System Control Block \(SCB\)](#) register, which triggers a system reset similar to pulling the reset pin low.

5.6 Probe Epoxy Casting

The circuitry on the probe had to be protected from the salt water while the electrodes were submerged, which was achieved using *Kristal 20* epoxy resin. Before casting the epoxy, the [RS-485](#) ports on the controller and probe were connected using a multicore cable, which connected their power, ground and the [RS-485](#) data lines, which can be seen in Figure 5.5. A casting mould was created using acrylic sheets, which are commonly used for epoxy moulds as they tend not to stick to the epoxy. The sheets were cut and secured using hot glue, as seen in Figure 5.6.



Figure 5.5: A top view of the probe casting mould, the controller and the connecting cable.

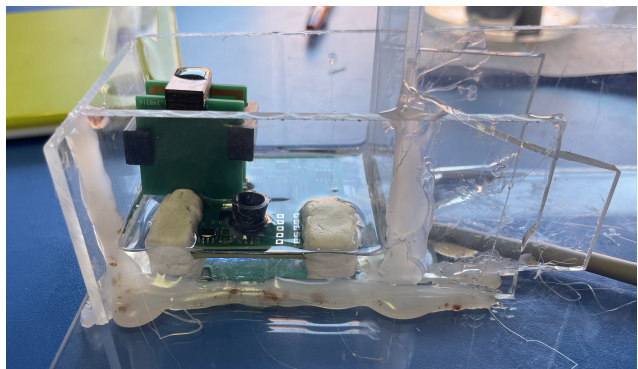


Figure 5.6: A side view of the probe casting mould showing the gold electrode spacers.

The gold electrodes were precisely spaced using 3D-printed spacers, which were attached during the casting process and removed once the epoxy had cured. Lastly, two areas of the probe still needed to be accessed: the programmer and [UART](#) ports and the titanium electrode ports. This would simplify

further testing and allow the titanium electrodes to be optimally spaced through experimentation instead of estimations. These areas were isolated using *Prestick*, a rubber-based reusable putty adhesive. The adhesive was removed after the epoxy had cured, allowing access to the aforementioned areas.

The probe was removed from the mould after the epoxy had cured, shown in Figure 5.7. The *Prestick* adhesive was relatively easy to remove, and the desired areas were still accessible, allowing the titanium electrode to be added. Titanium is challenging to solder, requiring a complex process and advanced machinery that was not available for this project [59]. Instead, thin copper wire was tightly wrapped around the last 5mm of the titanium electrode, which was folded over to secure the copper wire, as shown in Figure 5.8. This configuration made connecting the electrodes to their ports easy using standard soldering and provided a continuous connection between the probe and the titanium electrode.

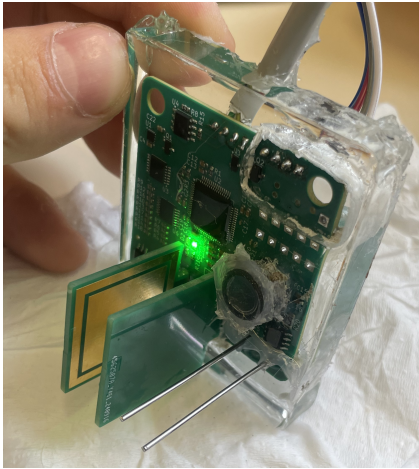


Figure 5.7: The probe after the epoxy casting process with the titanium electrodes and pressure sensor's flexible membrane attached.

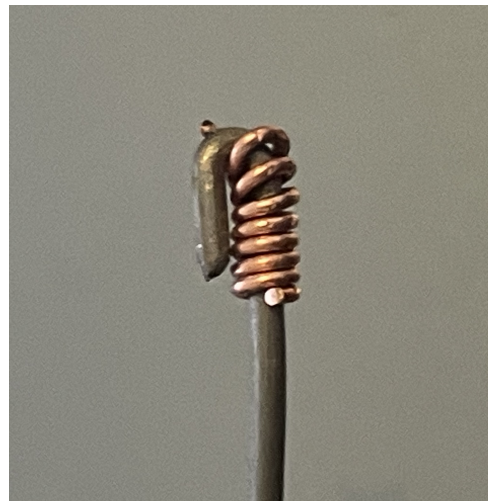


Figure 5.8: A close-up of the titanium electrode with the copper wire attached.

The unevenness of the mould and the hot glue created some rough edges along the epoxy. These could be laser cut to a smooth finish for the final product, but this was considered unnecessary for the experiments conducted in this project.

Lastly, hot glue was used to attach a flexible membrane to the pressure sensor's protective casing. The membrane was taken from the packaging of the gold electrode PCBs as it was readily accessible and had the required flexibility and durability to prove the concept. The final device would require further investigation into a more suitable material. The protective casing was also coated in a thin layer of hot glue as the 3D printing process used to create it had a small probability of being porous.

Chapter 6

Salinometer Evaluation and Testing

6.1 Overview

Several tests were conducted to evaluate the salinometer. The tests experimentally verified the accuracy of the individual components, evaluated the salinometer's interaction with saltwater samples and determined its ability and accuracy in measuring salinity. The tests were conducted in two phases because some required access to the board's circuitry and test points, while others required the probe to be exposed to salt water, which could only happen after the probe was cast in epoxy. The first phase involved evaluating the [DAC](#), [ADC](#), calibration resistor and resistance measuring accuracy which is covered in Section [6.3](#) to Section [6.6](#).

After the first testing phase, the probe was cast into epoxy resin as described in Section [5.6](#), which allowed the second phase to commence. First, the pressure sensor was tested, and it was confirmed to be working as expected, returned accurate temperature and pressure readings. The second phase involved establishing a voltage-resistance relationship for the salt water, a voltage-to-conductivity relationship for both electrodes and finally, the salinometer's ability to measure salinity, which is covered in Section [6.7](#) to Section [6.10](#). No corrosion nor electrolysis was noticed during these tests, proving that the choice of materials and the bidirectional measurements were effective at preventing these issues. A summary of these tests is shown in Table [6.1](#), and each test is discussed in further detail in its relevant section.

Table 6.1: A summary of the evaluation and testing of the salinometer.

Sec.	Test Description	Result Metric	Ideal Result	Measured Results
6.3	The minimum and maximum voltage output of the DAC between $0V$ and $V_{DD} = 3,3V$	Range	$0 - 3,3V$	$0 - 2,59V$
6.3	The gain and offset of the output voltage of the DAC relative to the instructed voltage	Gain	1,0	0,9837
		Offset	$0,0V$	0,0070V
6.4	The gain and offset of the voltage measured by the ADC relative to the voltage measured by the multimeter	Gain Offset	1,0 $0,0V$	0,9877 0,0082V
6.5	The resistance of the calibration resistor	Resistance	5Ω	$5,00\Omega$

Continued on next page

Table 6.1: A summary of the evaluation and testing of the salinometer. (Continued)

6.6	The gain and offset of the resistance measured by the salinometer relative to the resistance measured by the multimeter	Gain Offset	1 0Ω	1,0000 $0,0000\Omega$
6.7, 6.8	The repeatability of voltage sweep measurements, the difference between measurements of different samples, and the accuracy of the calculated salinity	Repeatability Differentiability Accuracy	Identical Clear Accurate	Within 10% Clear Inaccurate
6.9	The repeatability of individual voltage measurements, the difference between measurements of different samples, and the accuracy of the calculated salinity	Repeatability Differentiability Accuracy	Identical Clear Accurate	Within 10% Clear Within 4 PSU
6.10	The repeatability of AC voltage measurements, the difference between measurements of different samples, and the accuracy of the calculated salinity	Repeatability Differentiability Accuracy	Identical Clear Accurate	Untested Unclear -

6.2 Testing Apparatus

Voltage and resistance measurements were taken on the probe using a bench multimeter. The most accurate multimeter available was a *Keysight Technologies* U3401A, shown in Figure 6.2, which had voltage accuracy of 0,02% and resistance accuracy of 0,1%. In order to test the probe PCB, voltage probes were connected to the test points, shown in Figure 6.1, or they were connected directly to the components.

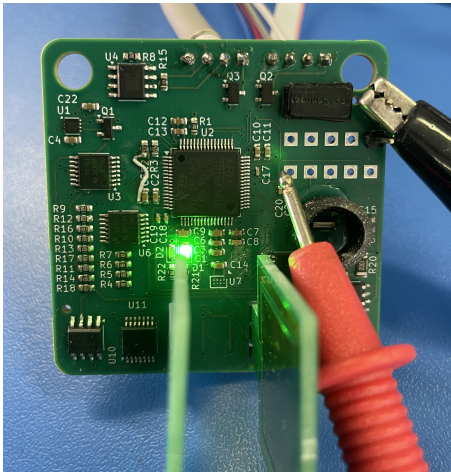


Figure 6.1: The salinometer probe with multimeter cables attached to a test point and ground.



Figure 6.2: The bench multimeter used for the tests displaying a voltage reading.

6.3 DAC Voltage Range and Accuracy

The transistor buffer configuration explained in Section 6.3 has one disadvantage: the output voltage of the system is limited by the transistor's V_{BE} where the highest possible voltage output is $V_{DD} - V_{BE}$. According to the transistor's [data sheet](#), the buffered output should be limited to $3,3V - 0,6V = 2,7V$ when conducting $0A$ and $3,3V - 0,75V = 2,55V$ when conducting the circuit's maximum current of $33mA$. In order to assess the range and accuracy of the [DAC](#), it was instructed to output voltages from $0V$ to $V_{DD} = 3,3V$ in intervals of 64-bit. The output voltage was measured at the base and emitter of the transistor, with no load and a maximum load of 100Ω . The results were graphed and shown in Figure 6.3 and Figure 6.4.

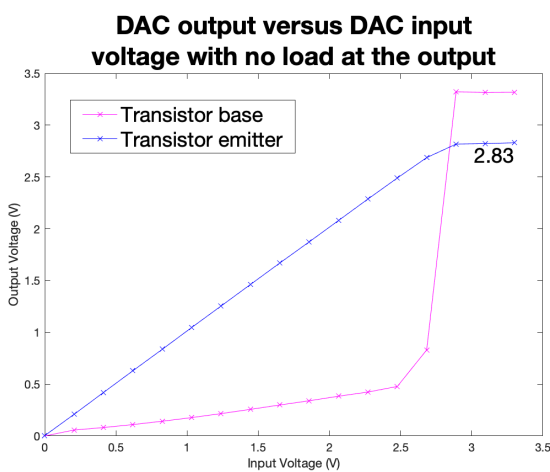


Figure 6.3: The input voltage versus the output voltage of the [DAC](#) with no load.

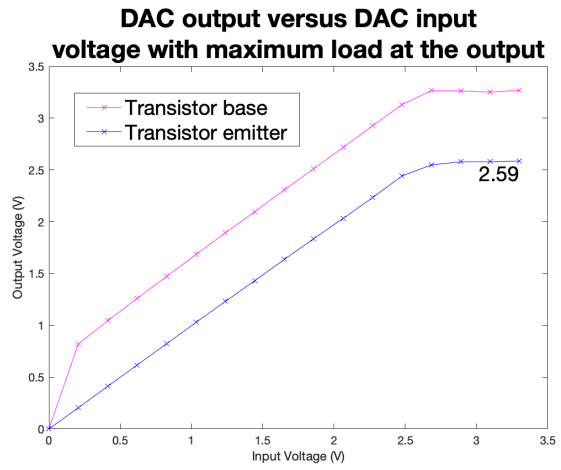


Figure 6.4: The input voltage versus the output voltage of the [DAC](#) with the maximum load of 100Ω .

The voltage drop due to V_{BE} can clearly be seen on Figure 6.4. The unloaded output voltage reached $2,83V$, and the loaded output voltage reached $2,59V$, which were slightly higher than the predicted limits.

An alternative attempt was made to achieve a higher voltage output using the [DAC](#)'s internal voltage reference of $1,21V$ multiplied by a gain of 4, resulting in a reference of $4,84V$. As expected, this did not increase the output voltage; the base of the transistor continued to measure $3,3V$ and the emitter $2,83V$ while unloaded.

Due to the voltage limitations, the [DAC](#) was limited to $2,6V$ for future testing and implementation. When excluding the voltage readings above $2,6V$, the [DAC](#) achieved a gain of $0,9837V/V$ and an offset $+0,0070V$ between the input voltage and measured voltage under maximum load.

6.4 ADC Accuracy

The [ADC](#) was tested by measuring a range of voltages produced by the [DAC](#) and comparing them to the multimeter's measurement. The [ADC](#) was configured in 12-bit mode, with each measurement taking 15 [ADC](#) clock cycles, equivalent to $250ns$ with the $16MHz$ system clock. 5 measurements

were taken and averaged for each voltage outputted by the **DAC** to increase the accuracy of each measurement. The results were graphed and shown in Figure 6.5.

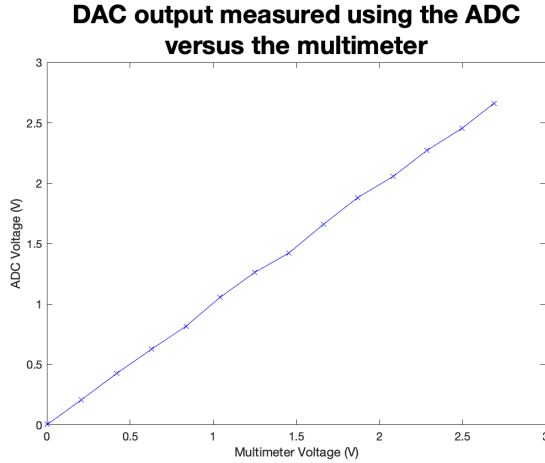


Figure 6.5: The voltage output by the **DAC** measured by a multimeter versus by the **ADC**.

The **ADC** achieved a gain of $0,9877V/V$ and an offset of $0,0082V$ compared to the multimeter.

6.5 Calibration Resistance

The multimeter measured the calibration resistor by directly connecting its probes to the four parallel resistors. The calibration resistor was electrically disconnected from the rest of the circuit during the measurement. The calibration resistance was specified to be $5\Omega \pm 0,25\%$; thus, its actual value could range between $4,9875$ and $5,0125\Omega$.

The multimeter measured the calibration resistor to be $5,25\Omega$. However, the multimeter probes measured $0,25\Omega$ when short-circuited. Thus, the actual resistance was calculated as $5,00\Omega$. It should be noted that the multimeter can only display to the nearest $0,01\Omega$. Thus, the actual resistance could range from $4,995\Omega$ to $5,005\Omega$, and more precise equipment would be required to obtain a more accurate measurement.

6.6 Resistance Measuring Accuracy

The probe's accuracy in measuring resistance was determined by comparing its calculated resistance to the multimeter's measurement of a given resistor. The probe calculated resistance by measuring the voltage drop across the resistor attached between the titanium electrode ports and the calibration resistor. Then, it calculated its resistance per Equation 4.4 to Equation 4.6.

For this test, the probe measured resistance using two methods: one with a single voltage provided by the **DAC** of $V_{DD}/2 = 1,65V$ and one with voltage sweep from the **DAC** with 50 samples. In the latter case, the resistances were calculated for each sample and averaged. At low voltages, single-bit errors caused significant changes in the calculated resistance, which were avoided by limiting the voltage sweep to between $0,3V$ and $2,6V$. The resistors used had a range of 0Ω , or a short-circuit, to 10Ω .

as this is the expected range for the gold electrodes. The results of the voltage sweep versus the multimeter test are shown in Figure 6.6.

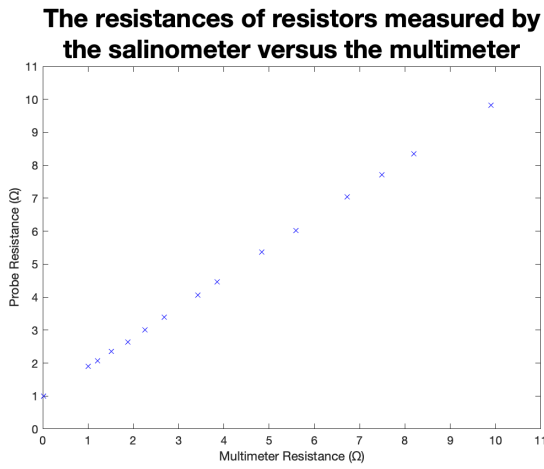


Figure 6.6: The resistance measuring test.

The resistances of resistors measured by the salinometer versus the multimeter using the corrected equation

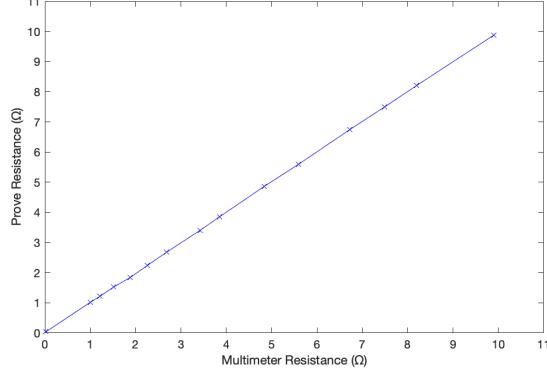


Figure 6.7: The resistance measuring test using the corrected equation.

The single voltage and voltage sweep methods were perfectly correlated with an r^2 value of 1,0000. However, there was a clear error between the probe's and the multimeter's measurements. This error was assumed to be due to the unaccounted resistance of the switches and the traces. While these values could be measured and included in the equation, a more efficient and arguably more accurate method would be to generate an equation of best fit and use it to calculate the correct resistance.

To determine the general formula of the equation of best fit, Equation 5.1 with the electrode resistance R_E and the calibration resistance R_C , was adjusted to include r_e , which represents the unknown resistance of the switches and traces as shown in Equation 6.1. R_C , R_1 and r_e were condensed into the standard rational function coefficients p and q as shown in Equation 6.2. Finally, the equation was rearranged to give the electrode's resistance in terms of the measured voltage ratio as shown in Equation 6.2.

$$V_{ratio} = \frac{\frac{R_E + r_{e1}}{R_E + R_1 + r_{e2}}}{\frac{R_C + r_{e3}}{R_C + R_1 + r_{e4}}} = \frac{R_E + r_{e1}}{R_E + R_1 + r_{e2}} \times \frac{R_C + R_1 + r_{e4}}{R_C + r_{e3}} \quad (6.1)$$

$$V_{ratio} = \frac{p_1 R_E + p_2}{R_E + q_1} \quad (6.2)$$

$$R_E = \frac{p_2 - q_1 V_{ratio}}{V_{ratio} - p_1} \quad (6.3)$$

The Equation 6.2 of best fit was confirmed using MATLAB, which gave the values $p_1 = 17,4687$, $p_2 = 18,4643$ and $q_1 = 91,8315$ with an r^2 value of 1,0000. The corrected resistance values were obtained from the previous data set by reversing the previous formula and applying Equation 6.3 to

the voltage ratios. These results were graphed and are shown in Figure 6.7 and have a gain of 1,0000 and an offset of 0,0000. Note that this correction equation is only valid when R_1 is 100Ω and separate equations will need to be generated should different values of R_1 be needed.

6.7 Voltage Sweep Repeatability

The following tests investigate a method for producing repeatable voltage measurements of a saltwater sample. In order to conduct these tests, the probe was cast into epoxy as described in Section 5.6.

The tests were configured with parameters such as which electrodes to use, the voltage sample count, the ADC sample count and the DAC range. Due to a circuit error discovered after the epoxy casting, the gold electrodes could only be used with the fringe guard. Thus, the effectiveness of the fringe guard was unable to be tested. Each voltage sweep results were transmitted over UART to a computer, where they were processed using Microsoft Excel and MATLAB to generate graphs and metrics.

The first test was a voltage sweep performed both forwards and in reverse with increasing and decreasing DAC voltages respectively. The test was configured with the gold electrodes and the fringe guard, 50 voltage samples, 2 ADC samples and a voltage range of 0 – 2,6V. It was performed on a salt water sample of unknown salinity around 30 PSU. Ideally, the two sweeps should have been identical. However, they were not, as shown in Figure 6.8.

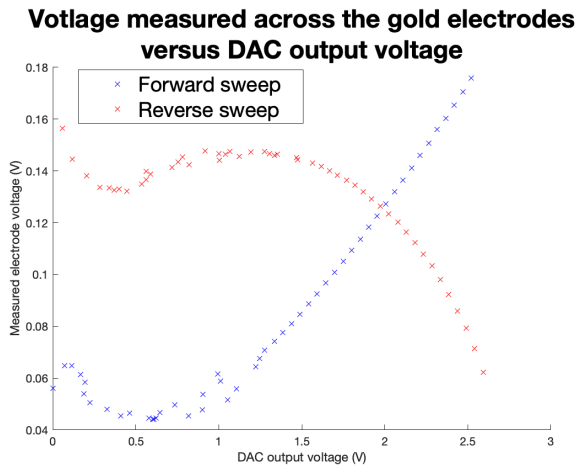


Figure 6.8: Voltage sweep repeatability test 1 with gold electrodes and the fringe shield, a voltage range of 0 – 2,6V, and 50 samples taken of salt water sample of unknown salinity.

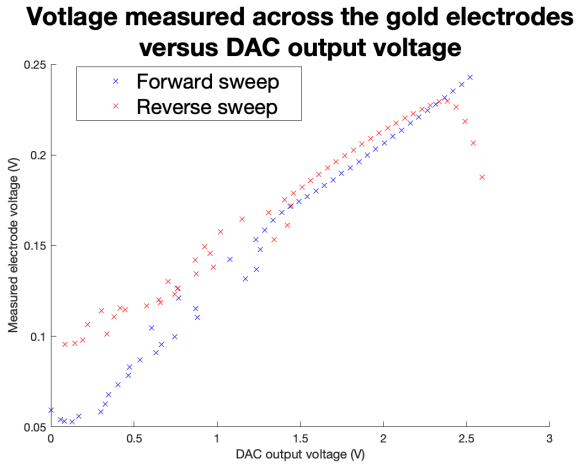


Figure 6.9: Voltage sweep repeatability test 2 with draining and resetting the DAC between each voltage sample.

To further investigate the inconsistency, the DAC was reset to 0V before it was set to the desired voltage for each sample. It should be noted that the DAC reset added a slight delay between each voltage sample of around 10ms. While this did make the forward and reverse sweeps more similar, as shown in Figure 6.9, the initial voltage lag of the reverse sweep on the right hand-side of the graph was still present.

It was theorised that the measurements of the water briefly altered its properties, which in turn altered the proceeding measurements. This alteration was unlikely to be a capacitive effect, as the

measurements were taken bidirectionally, which would have dissipated any built-up charge. It was possible that the voltage was dissociating the dissolved material into ions, allowing the charges in the salt water sample to move more freely and alter the measurement [39]. However, determining exactly what caused the alteration was beyond the scope of this project.

Instead, to further investigate this, a test was conducted taking priming measurements at the maximum voltage of 2,6V before capturing the actual measurements. The priming caused the actual measurements in both directions to start high and progressively move to their predicted paths, as shown in Figure 6.10.

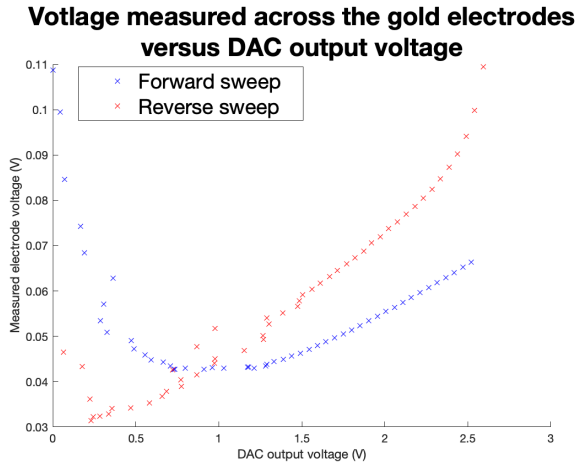


Figure 6.10: Voltage sweep repeatability test 3 with 25 priming measurements taken before the actual measurement.

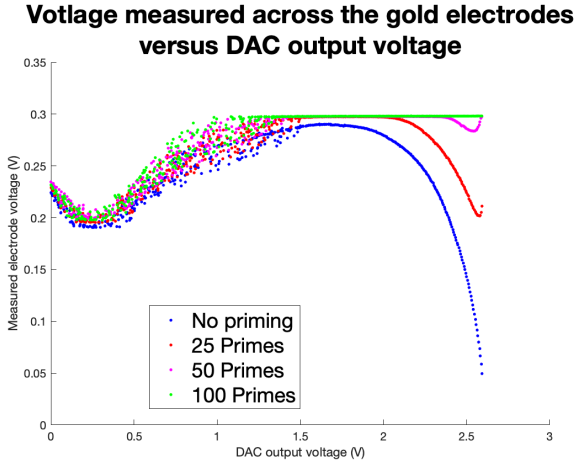


Figure 6.11: Voltage sweep repeatability test 4 with a varying number of priming measurements and the actual measurement taken as reverse voltage sweeps with 500 voltage samples.

This result supported the theory that the measurements were affecting the water. The next test varied the number of priming measurements and used 500 voltage samples to increase the curve's resolution, as shown in Figure 6.11. It should be noted that the voltage measurement effectively clipped at 0,3V as the output of the $11 \times$ gain op-amp reached $0,3 \times 11 = 3,3V$, which is the maximum voltage it can output.

While it was theoretically possible to perfectly prime a measurement, it was considered impractical, and it was also unlikely that the priming would have zero impact on the actual measurements. Thus, voltage priming was not considered a viable solution for making repeatable measurements. These results also indicated that a voltage measurement could be vulnerable to the priming effect from the previous measurement, which would cause undesirable effects. Thus, an alternative method was needed to take the measurements.

It was noticed that the priming effect decreased over time, allowing the voltage sweeps in Figure 6.10 to return to their expected curves. A new theory stemmed from this that the water could relax from a primed state over time. To test this, a delay, or relaxation time, was added between voltage samples, during which no voltage was applied to the electrodes. The first test used relaxation times of 2s and 500ms and stirring to cycle the water between the electrodes. With a 2s relaxation time, the forward and reverse voltage sweeps were near identical, as shown in Figure 6.12. However, with a 500ms relaxation time, there was a clear difference and the same initial voltage lag shown in Figure 6.9.

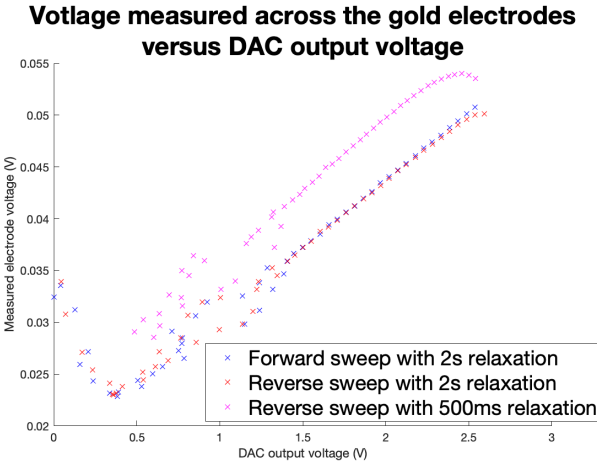


Figure 6.12: Voltage sweep repeatability test 5 with a varying amount of relaxation time before each measurement was taken and 50 samples.

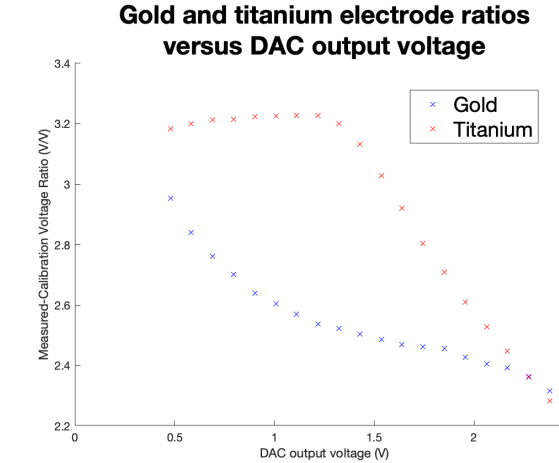


Figure 6.13: Voltage sweep repeatability test 6 with the difference between the titanium and gold electrodes.

This test concluded a valid method of measuring a voltage sweep, which used a relaxation time of 2s between each voltage sample. This method allowed the titanium electrodes' length and spacing to be experimentally configured such that they could use the same R_1 value of 100Ω as the gold electrodes. Iterative testing revealed that a length of 30mm and a spacing of 6mm used most of the 0V to 0,3V range available to the electrodes. A test comparing the titanium and gold electrodes was performed using a relaxation time of 2s, shown in Figure 6.13. The results showed that the gold electrodes followed the same curve that Reference [38] found, while the titanium electrodes did not. The reason for this is unknown; it was theorised that the titanium electrodes' fringing effect and conductivity difference were the cause, but this required further investigation.

The investigation into determining a repeatable voltage sweep necessitated two more tests: the repeatability of the sweep on the same sample and the differentiation between samples. The former involved taking two voltage sweeps of two different saltwater samples of unknown but different salinities, shown in Figure 6.14. These results showed that the voltage sweeps were approximately grouped by salinity, allowing for a clear differentiation between the two samples despite the noise in the measurements.

Next, an individual measurement's repeatability was further investigated by taking four identical voltage sweeps of the same saltwater sample. The results, shown in Figure 6.15, found that the measurements were approximately grouped. However, it was noticed that the voltage sweeps drifted upwards with each successive measurement. A higher voltage sweep indicated a higher resistance, lower conductivity, and thus a lower salinity. This was likely due to the previous sweep affecting the proceeding one, similar to the priming effect. A test that could isolate both issues would be replacing the water between the electrodes during the voltage sweep. This could be achieved using a pump and a large volume of water of known salinity, similar to how Ocean Exploration's CTD operate. However, this apparatus was not available to this project.

It was noticed that there was a measurement inconsistency of the voltage samples below 1,5V, which is visible in Figure 6.12. However, the same inconsistency was present in the measurement and calibration reading. Thus, it was likely due to noise in the ADC or op-amp. A similar inconsistency was present

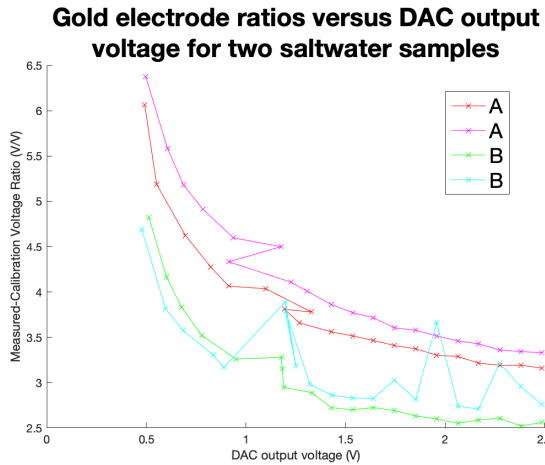


Figure 6.14: Voltage sweep repeatability test 7 with 4 identical tests of 20 samples with 2s of relaxation time between measurements.

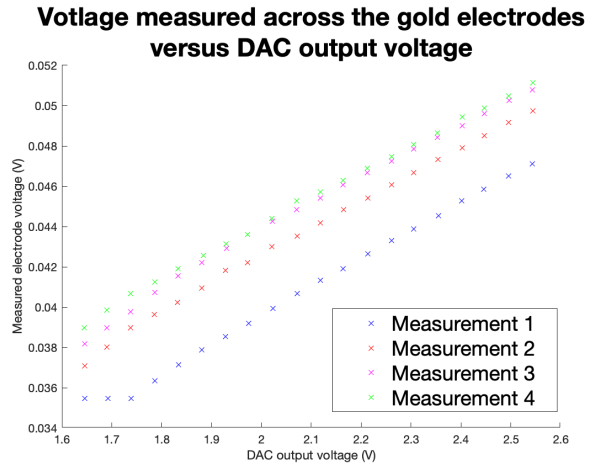


Figure 6.15: Voltage sweep repeatability test 8 with 4 identical tests of 20 samples with 2s of relaxation time between measurements.

at the end of the voltage range, shown in Figure 6.13, likely due to the voltage lag of the reverse sweep. To allow for a more straightforward analysis, these voltages were excluded.

6.8 Voltage to Conductivity Mapping

The following investigation aimed to determine the relationship between a saltwater sample's voltage sweep and conductivity. This required samples of known salinity, which were created by mixing sea salt and distilled water. A handheld salinometer, accurate to 0,1 PSU, was used to measure the samples, which were 24,4, 29,1, 32,9 and 34,8 PSU.

In order to correctly assess the relationship between the voltage and conductivity, the probe had to calibrate on a standard solution of 35 PSU at 15°C and 0dbar. 34,8 was the closest value attainable to the required PSU using the equipment available. This sample was placed in a fridge and cooled to below 15°C, then removed and placed at room temperature where it warmed up. Once the sample reached approximately 15°C, four voltage sweeps were taken with the gold and titanium electrodes using 20 voltage samples and 2s of relaxation, shown in Figure 6.16 and Figure 6.17.

The gold electrode test showed a similar result to Figure 6.14, where the measurements had the same shape and were approximately grouped, increasing with each successive test. However, the titanium electrode test shows different results, appearing to have two different curves. The samples taken below 1,4V appeared concave, while those above 1,4V appeared convex, which was confirmed not to be due to the voltage clipping at 0,3V. It was theorised that this was due to the fringing effect of the titanium electrodes, which were overlaid with the resistance-voltage curve of the saltwater sample. However, this could not be verified, as the gold electrodes could not be tested without the fringe guards. Thus, the fringing effect could not be further studied.

Similar measurements were taken of the 24,4 PSU and 29,1 PSU samples, shown in Figure 6.18 to Figure 6.21, to allow for a comparative analysis. These tests were not conducted at 15°C, which required their temperatures to be recorded and corrected for in the salinity equation. All the tests were conducted at 0dbar. Thus, pressure did not need to be corrected.

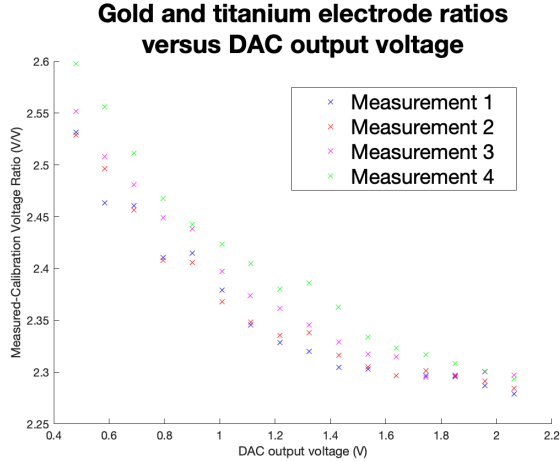


Figure 6.16: Conductivity mapping test 1 with 4 tests using the gold electrodes and the fringe guard tests taken of a 34,8 PSU sample at 15,0°C.

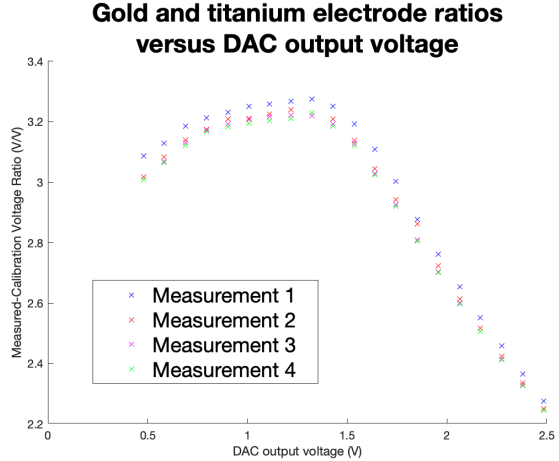


Figure 6.17: Conductivity mapping test 2 with 4 tests using the titanium electrodes taken of a 34,8 PSU sample at 15,0°C.

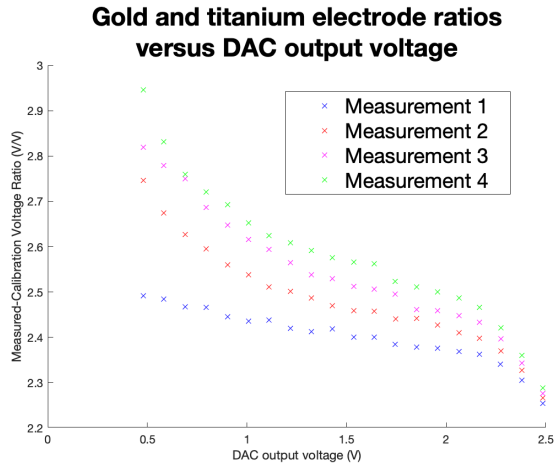


Figure 6.18: Conductivity mapping test 3 with 4 tests using the gold electrodes and the fringe guard tests taken of a 24,4 PSU sample at 21,7°C.

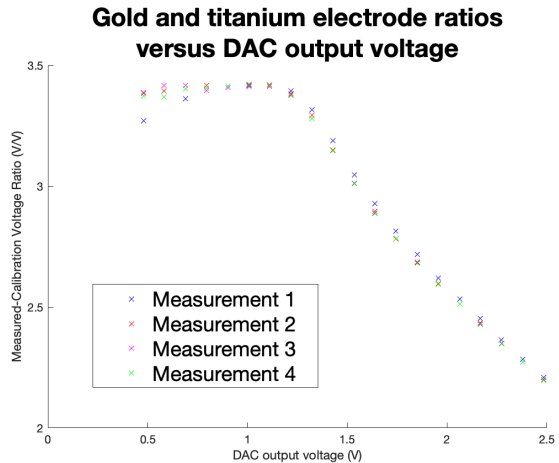


Figure 6.19: Conductivity mapping test 4 with 4 tests using the titanium electrodes taken of a 24,4 PSU sample at 21,7°C.

These results showed a similar trend to the tests performed on the standard solution with the gold and titanium electrodes. The gold electrodes continued to show variations between successive measurements, and it was noted that the titanium electrodes showed excellent consistency above 1,4V.

To determine salinity, either a mathematical relationship between the curves and their salinity could be generated, or a metric from the equation of best fit could be taken as the effective conductivity. The latter method was considered more straightforward and was attempted first. The logical equation of best fit was a hyperbolic function, where the voltage ratio, measured voltage, and electrode resistance would approach infinity as the conductivity and salinity approach zero.

The ideal hyperbole function $y = \frac{a}{x}$ was modified to include an offset $y = \frac{a}{x} + c$, as even with infinite conductivity, there would still be some resistance and voltage drop expected due to the switches and traces in the probe. The equation parameters were calculated using MATLAB and graphed using the first measurement of each sample, shown in Figure 6.22 and Figure 6.23. The abnormalities at the

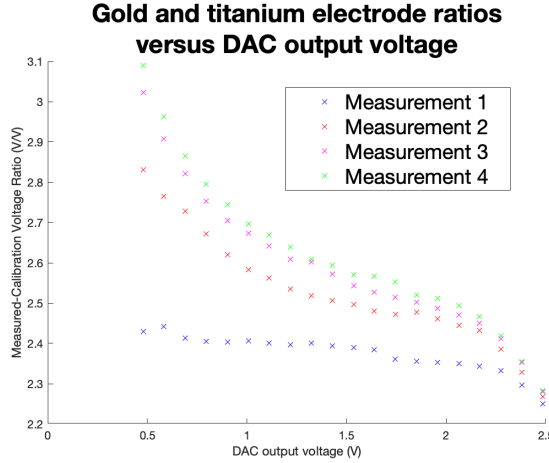


Figure 6.20: Conductivity mapping test 5 with 4 tests using the gold electrodes and the fringe guard tests taken of a 29,1 PSU sample at 20,2°C.

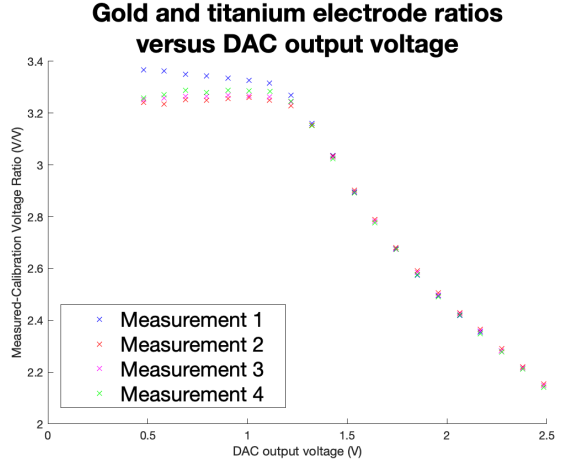


Figure 6.21: Conductivity mapping test 6 with 4 tests using the titanium electrodes taken of a 29,1 PSU sample at 20,2°C.

higher voltages of gold electrode tests were removed, and the concave section of the titanium electrode tests below 1,4V was removed to allow for a more straightforward analysis.

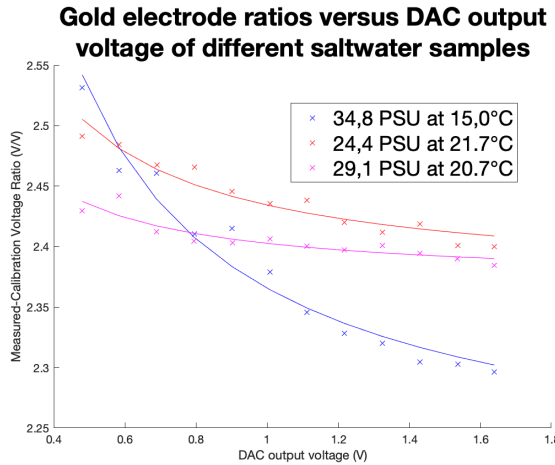


Figure 6.22: The gold electrode tests of known samples with hyperbolic curves of best fit generated.

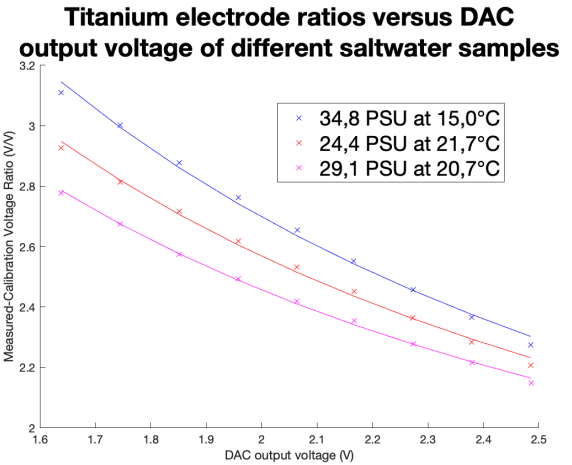


Figure 6.23: The titanium electrode tests of known samples with hyperbolic curves of best fit generated.

The gold and titanium electrode tests of the 24,4 and 29,1 PSU samples measured at similar temperatures showed a logical difference between their voltage sweeps, where the lower salinity sample had a higher voltage ratio. However, the 34,8 PSU did not follow this, likely due to its temperature change, which would have lowered its conductivity [6].

The gain value a was calculated for each of these curves. Higher salinities appeared to have lower a values; thus, they were inverted before calculating salinity. These values and their corresponding salinities are shown in Table 6.2. While these results return relatively higher values for higher salinity samples, they were required to be more accurate. Attempts were made by raising the a value to different powers, using the c value, and linear offsets to a , but none resulted in correct salinity values. It should be noted that multiplying the a was ineffective, as salinity is calculated based on the ratio of

two different a values.

Table 6.2: The gain values a of the hyperbolic curve of best fits and the calculated salinities.

Electrode	Sample Salinity (PSU)	Gain Value a	Temperature (°C)	Calculated Salinity (PSU)
Gold	34,8	0,1631	15,0	-
Gold	24,4	0,0656	21,7	84,9
Gold	29,1	0,0320	20,2	226,6
Titanium	34,8	4,0506	15,0	-
Titanium	24,4	3,4400	21,7	35,7
Titanium	29,1	2,9851	20,2	43,4

This investigation concluded that the probe could detect a clear and logical difference between salinity samples, but calculating salinity using the measurements proved inaccurate. While further investigation could be conducted into determining a mathematical relationship between the curves and their respective conductivities, it was considered viable only with more accurate data attained through the previously mentioned method of pumping water over the electrode. Thus, alternative methods were investigated.

6.9 Individual Voltage Measurements

A second approach, similar to that of Reference [40], was investigated, which used a single voltage measurement to calculate the salinity. While this would prevent any impact of the priming effect, a single measurement is highly vulnerable to noise and errors, which could cause inaccuracies in the salinity calculation. Tests were conducted with the gold electrodes and the fringe guard with the DAC set at 1,65V, as this voltage appeared to be the most stable from the previous tests. Similar to Section 6.8, a standard solution of 34,8 PSU was measured at 15°C and 0dbar. Then, measurements of the other three samples were taken, and their temperatures were recorded. The results are shown in Table 6.3.

Table 6.3: The individual voltage measurements taken of different salt water samples.

Sample Salinity (PSU)	Voltage Ratio (V/V)	Calculated Resistance (Ω)	Temperature (°C)	Calculated Salinity (PSU)
34,8	2,178	11,87	15,0	-
24,4	2,320	12,79	23,7	24,9
29,1	2,288	12,62	23,7	25,5
32,9	2,058	11,06	23,7	32,2

The voltage ratio was calculated for each sample, followed by its resistance using the correct resistance equation, Equation 6.3, determined in Section 6.6. The salinity was then calculated using the resistances.

Calculating conductivity using resistance was a scalar operation and thus was omitted as it does not affect the salinity calculation, as previously mentioned. While these values proved more accurate in estimating salinity than the voltage sweep, they were inconsistent and subject to noise and error.

6.10 AC Voltage Measurements

A third approach, similar to that of Reference [41], was investigated, which used an **AC** sine wave to measure the saltwater's response. A sine wave was generated by writing precalculated values of a half sin wave to the **DAC** and changing the current direction between the electrodes every half wave, which gave the effect of a full sine wave centred around ground. **ADC** measurement were taken every time the **DAC** voltage was updated. A slight, configurable delay was added between each **DAC** updated to allow the frequency of the sine wave to be controlled. It should be noted that the probe was optimised for measuring **Direct Current (DC)** voltages, which required capacitors connected in parallel with the electrodes, which could not be removed after the probe was cast in epoxy. These capacitors likely affected the saltwater's measured response.

A sine wave test was performed on the 32,9 **PSU** sample using the titanium electrodes, shown in Figure 6.24. Due to the circuit errors previously mentioned, the gold electrodes could not perform this test. The sample had a phase delay in response to the sine wave. However, when the sine wave crossed 0V, the response would return to 0V as well. This was assumed to be due to the **DAC** draining the voltage from across the electrode when it crossed ground. Additionally, the amplitude of the sample's response appeared to migrate indicating that it had not stabilised.

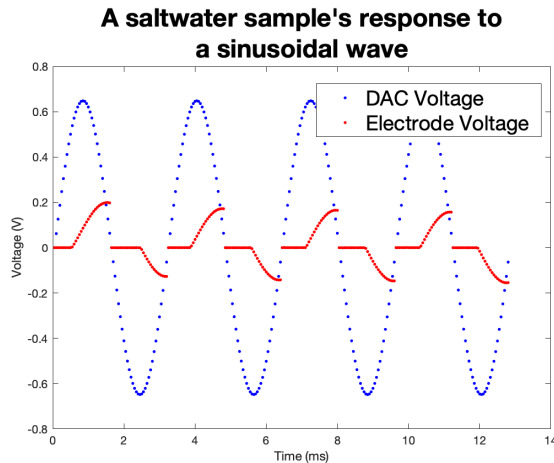


Figure 6.24: **AC** test 1 with a 4 sine waves centred at 0V.

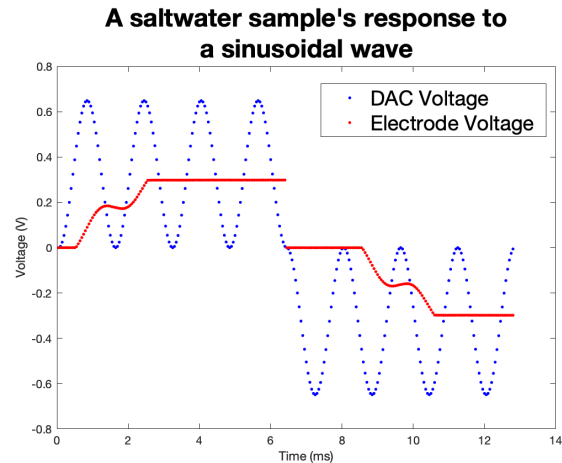


Figure 6.25: **AC** test 1 with a 4 sine waves centred at 1,65V and 4 sine waves centred at -1,65V.

A second test was conducted with the sine wave centred at $V_{CC}/2 = 1,65V$, which prevented the **DAC** from draining the voltage from the electrodes. The sine waves were repeated in both directions to prevent excessive corrosion of the electrode. The results, shown in Figure 6.25, show the response of the sine wave saturates with a similar effect to the priming experienced with the voltage sweeps. Thus, this test was considered not viable for salinity calculation.

Further tests centred at 0V were conducted on the 34,8 and 24,4 **PSU** samples. To allow the drift of

the peaks seen in Figure 6.24 to settle, 75 sine wave measurements were performed before the actual measurement was taken, shown in Figure 6.26 and Figure 6.27.

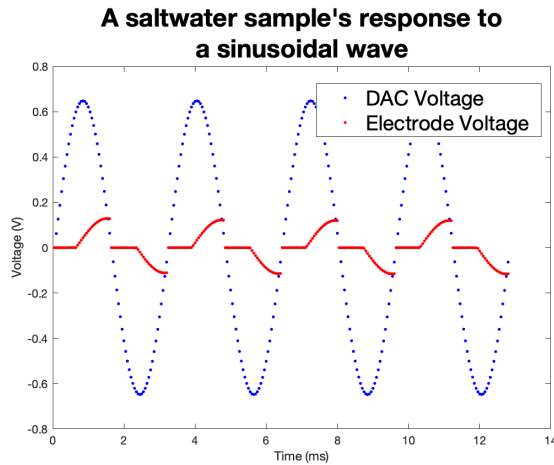


Figure 6.26: AC test 1 with a 4 250Hz sine waves centred at 0V on a 34,8 PSU sample.

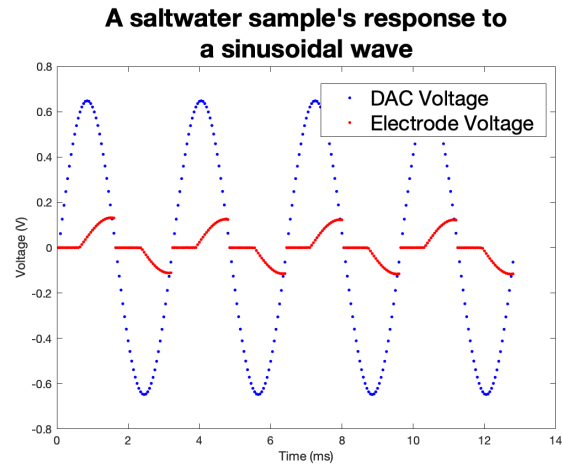


Figure 6.27: AC test 1 with a 4 250Hz sine waves centred at 0V on a 24,4 PSU sample.

These tests showed no discernable difference between the amplitude and phase of the two samples. This was likely due to the added capacitors affecting the response, and would need to be further investigated by first removing them before casting the probe into epoxy. Unfortunately, the time limitations of the project prevented this from being attempted.

Chapter 7

Conclusions

This project presented the development of a prototype electrical conductivity-based sensor and investigated its feasibility. The prototype was successfully designed and constructed with a separate probe for taking measurements and a controller for user inputs and displaying results. The probe was able to measure resistance with high accuracy, and it successfully demonstrated a controller-probe communication protocol.

The probe investigated three methods of measuring the electrical conductivity of a solution: voltage sweeps, **AC** voltage, and individual measurements. Voltage sweep measurements were subject to drift due to the individual measurement altering the solution and affecting the subsequent measurements. This caused difficulties in determining the salinity of the solution and required further investigation and tests to assess its viability.

AC voltage measurements were unsuccessful as the probe was optimised for **DC** measurements, causing the response of the saltwater sample to be interfered with by a capacitor on the probe. The probe could not be adjusted due to it being cast in epoxy. Thus, the feasibility of **AC** tests requires further investigation.

Individual measurements were shown to be the most accurate, reporting salinities within 4 **PSU** of the expected value. However, this method was vulnerable to noise and errors and has poor repeatability.

In conclusion, this project proved critical concepts of the probe's, controller's and electrodes' designs and the board-to-board communication. Additionally, the investigation into the conductivity measurement methods provided valuable insights into the challenges and potential solutions for the probe's future development.

Chapter 8

Recommendations

Further investigation of the methods of conductivity measurements was required. The voltage sweep method was vulnerable to individual measurements when adjusting the saltwater sample. To avoid this, using a water pump to circulate the water during the measurement is recommended. This setup would require a large volume of water of known salinity to be used, which would present additional challenges when calibrating the probe with the 35 PSU standard solution at 15°C and 0dbar.

The probe was not designed for measuring AC voltages. However, altering the probe to remove the capacitor that was likely interfering with the measurement would allow for a further investigation into AC voltage's feasibility. Additionally, a future iteration of the probe could be explicitly designed to measure AC voltages and determine its feasibility.

The attachment of the gold electrodes to the probe PCB was suboptimal, breaking on two occasions during the project. An alternative method of attaching them would be using a slot joint [60], where a slot could be cut into the probe and the electrodes, allowing them to slide into each other and be soldered in place on both sides, which would potentially be more robust. This design would make it challenging to have more than two connections to the electrode, but it could allow the probe to be thinner and taller, allowing it to fit down a smaller diameter ice core.

The controller proved successful in all its requirements, but a more user-friendly interface and housing would benefit the final device. A housing could be 3D printed to make the device easier to handle, more aesthetically pleasing, and protect it from the elements. Additionally, the 7-segment displays could be replaced with a Liquid Crystal Display (LCD), allowing for more detailed and clear information to be displayed to the user.

Bibliography

- [1] National Snow and Ice Data Center, “Ice sheet quick facts,” 2024.
- [2] National Snow and Ice Data Center, “Ice shelves,” 2024.
- [3] National Oceanic and Atmospheric Administration Ocean Explorer, “Arctic exploration 2002,” 2002.
- [4] NASA Earth Observatory, “Antarctic sea ice,” 2021.
- [5] A. E. Hogg, L. Gilbert, A. Shepherd, A. S. Muir, and M. McMillan, “Extending the record of antarctic ice shelf thickness change, from 1992 to 2017,” *Advances in Space Research*, vol. 68, no. 2, pp. 724–731, 2021. 25 Years of Progress in Radar Altimetry.
- [6] R. H. Stewart, *Introduction to Physical Oceanography*. Texas A&M University Press, 2004.
- [7] R. F. HU Sverdrup, MW Johnson, *The Oceans, Their Physics, Chemistry, and General Biology*. New York: Prentice-Hall, 1942.
- [8] E. L. Lewis and R. G. Perkin, “Salinity: Its definition and calculation,” *Journal of Geophysical Research*, vol. 83, no. C1, pp. 466–478, 1978.
- [9] Y. Zheng, Y. Liu, J. Zhou, and Y. Wang, “Electrical conductivity of the global ocean,” *Earth, Planets and Space*, vol. 69, no. 1, pp. 1–10, 2017.
- [10] Sea-Bird Scientific, “What are the differences between salinity expressions in ppt, psu (practical salinity), and absolute salinity?,” 2024.
- [11] International Oceanographic Commission, “Teos-10: The international thermodynamic equation of seawater (teos-10) for temperature, salinity, density, sound speed, and other oceanographic variables,” *Manuals and Guides*, vol. 56, 2010.
- [12] Seabird Scientific, “How accurate is salinity measured by my ctd? what factors impact accuracy.”
- [13] F. J. Millero and A. Poisson, “International one-atmosphere equation of state of seawater,” *Deep Sea Research Part A. Oceanographic Research Papers*, vol. 28, no. 6, pp. 625–629, 1981.
- [14] S. Yueh, R. West, W. Wilson, F. Li, E. Njoku, and Y. Rahmat-Samii, “Error sources and feasibility for microwave remote sensing of ocean surface salinity,” *IEEE Transactions on Geoscience and Remote Sensing*, vol. 39, no. 5, pp. 1049–1060, 2001.
- [15] D. Malardé, Z. Y. Wu, P. Gross, J.-L. de Bougrenet de la Tocnaye, and M. L. Menn, “High-resolution and compact refractometer for salinity measurements,” *Measurement Science and Technology*, vol. 20, p. 015204, dec 2008.

- [16] S. Yang, J. Xu, L. Ji, Q. Sun, M. Zhang, S. Zhao, and C. Wu, “In situ measurement of deep-sea salinity using optical salinometer based on michelson interferometer,” *Journal of Marine Science and Engineering*, vol. 12, no. 9, 2024.
- [17] R. H. Byrne and F. T. Mackenzie, “Seawater,” *Encyclopædia Britannica*, 2024.
- [18] W. S. Wooster, A. J. Lee, and G. Dietrich, “Redefinition of salinity,” *Journal of Marine Research*, vol. 27, no. 3, 1969.
- [19] U.S. Geological Survey, “Water density,” 2018.
- [20] B. Kjerfve, “Measurement and analysis of water current, temperature, salinity, and density,” in *Estuarine hydrography and sedimentation* (K. Dyer, ed.), pp. 187–226, Cambridge: Cambridge University Press, 1983.
- [21] University of Washington Department of Oceanography, “A compilation of articles reporting research,” 1966.
- [22] H. Schmidt, S. Seitz, E. Hassel, and H. Wolf, “The density–salinity relation of standard seawater,” *Ocean Science*, vol. 14, no. 1, pp. 15–40, 2018.
- [23] C. T. Swift and R. E. McIntosh, “Considerations for microwave remote sensing of ocean-surface salinity,” *IEEE Transactions on Geoscience and Remote Sensing*, vol. GE-21, no. 4, pp. 480–491, 1983.
- [24] C. Gabarró, J. Font, A. Camps, M. Vall-llossera, and A. Julià, “A new empirical model of sea surface microwave emissivity for salinity remote sensing,” *Geophysical Research Letters*, vol. 31, no. 1, 2004.
- [25] The European Space Agency, “Mapping salty waters,” 2019.
- [26] R. Millard and G. Seaver, “An index of refraction algorithm for seawater over temperature, pressure, salinity, density, and wavelength,” *Deep Sea Research Part A. Oceanographic Research Papers*, vol. 37, no. 12, pp. 1909–1926, 1990.
- [27] O. A. Tengesdal, “Measurement of seawater refractive index and salinity by means of optical refraction,” Master’s thesis, University of Bergen, 2012.
- [28] Y. Liao, K. Yang, and X. Shi, “Theoretical study on simultaneous measurement of seawater temperature and salinity based on dual fiber interferometers combined with nonlinear decoupling algorithm,” *Measurement*, vol. 211, p. 112596, 2023.
- [29] G. R. C. Possetti, R. C. Kamikawachi, C. L. Prevedello, M. Muller, and J. L. Fabris, “Salinity measurement in water environment with a long period grating based interferometer,” *Measurement Science and Technology*, vol. 20, p. 034003, feb 2009.
- [30] L. V. Nguyen, M. Vasiliev, and K. Alameh, “Three-wave fiber fabry–pérot interferometer for simultaneous measurement of temperature and water salinity of seawater,” *IEEE Photonics Technology Letters*, vol. 23, no. 7, pp. 450–452, 2011.

- [31] Y. Zhao, J. Zhao, Y. Peng, R.-J. Tong, and L. Cai, "Simultaneous measurement of seawater salinity and temperature with composite fiber-optic interferometer," *IEEE Transactions on Instrumentation and Measurement*, vol. 71, pp. 1–8, 2022.
- [32] R. Somaraju and J. Trumpf, "Frequency, temperature and salinity variation of the permittivity of seawater," *IEEE Transactions on Antennas and Propagation*, vol. 54, no. 11, pp. 3441–3448, 2006.
- [33] B. Waltrip, S. Avramov-Zamurovic, and A. Koffman, "Inductance measurement using an lcr meter and a current transformer interface," in *2005 IEEE Instrumentationand Measurement Technology Conference Proceedings*, vol. 2, pp. 1005–1007, 2005.
- [34] K. A. Alhassoon, Y. Malallah, and A. S. Daryoush, "Complex permittivity and permeability extraction of ferromagnetic materials for magnetically tuned microwave circuits," *IEEE Journal of Microwaves*, vol. 1, no. 2, pp. 639–645, 2021.
- [35] P. Pattakos, A. Katsoulas, S. Angelopoulos, A. Ktena, P. Tsarabaris, and E. Hristoforou, "Development of an autonomous magnetic permeability sensor," *IEEE Transactions on Magnetics*, vol. 59, no. 2, pp. 1–4, 2023.
- [36] J. A. Ewing, "A magnetic balance for workshop tests of permeability," *Journal of the Institution of Electrical Engineers*, vol. 27, July 1898.
- [37] O. A. Tengesdal, B. L. Hauge, and L. E. Helseth, "Electromagnetic and optical methods for measurements of salt concentration of water," *Journal of Electromagnetic Analysis and Applications*, vol. 6, no. 6, 2014.
- [38] R. Benjankar and R. Kafle, "Salt concentration measurement using re-usable electric conductivity-based sensors," *Water Air and Soil Pollution*, vol. 232, no. 13, p. 13, 2021.
- [39] V. J. Ostendorp and D. J. Bord, *Inquiry into Physics*. Boston: Cengage Learning, 2020.
- [40] Autodesk Instructables, "Water salinity-meter : 7 steps."
- [41] J. Jonsson, K. Smedfors, L. Nyholm, and G. Thornell, "Towards chip-based salinity measurements for small submersibles and biologgers," *International Journal of Oceanography*, vol. 2013, p. 11, 2013.
- [42] Sea-Bird Scientific, "Conversion of pressure to depth," 2024.
- [43] T. L. Hill, *An introduction to statistical thermodynamics*. Courier Corporation, 1986.
- [44] A. Poisson and M. H. Gadhoumi, "An extension of the practical salinity scale 1978 and the equation of state 1980 to high salinities," *Deep Sea Research Part I: Oceanographic Research Papers*, vol. 40, no. 8, pp. 1689–1698, 1993.
- [45] G. T. Furukawa, J. L. Riddle, and W. R. Bigge, "The international practical temperature scale of 1968 in the region 13.81 k to 90.188 k as maintained at the national bureau of standards," *Journal of Research of the National Bureau of Standards-A. Physics and Chemistry*, vol. 77A, no. 3, pp. 309–322, 1973.

- [46] H. Preston-Thomas, “The international temperature scale of 1990 (its-90),” *Metrologia*, vol. 27, no. 107, pp. 3–10, 1990.
- [47] M. Solomentsev and A. J. Hanson, “Modeling current distribution within conductors and between parallel conductors in high-frequency magnetics,” *IEEE Open Journal of Power Electronics*, vol. 3, pp. 635–650, 2022.
- [48] S. Hwang and J. Shim, “A method for current spreading analysis and electrode pattern design in light-emitting diodes,” *IEEE Transactions on Electron Devices*, vol. 55, no. 5, pp. 1123–1128, 2008.
- [49] S.-R. Jeon, Y.-H. Song, H.-J. Jang, G. M. Yang, S. W. Hwang, and S. J. Son, “Lateral current spreading in GaN-based light-emitting diodes utilizing tunnel contact junctions,” *Applied Physics Letters*, vol. 78, pp. 3265–3267, 05 2001.
- [50] Jason, “Current spreading in long objects,” tech. rep., The MITRE Corporation, 7515 Colshire Drive, McLean, Virginia 22102-753, oct 2008. Approved for public release; distribution unlimited.
- [51] “What is the typical water conductivity range? | atlas scientific,” 2022.
- [52] F. Walsh, “Electrode reactions in metal finishing,” *Transactions of the Institute of Metal Finishing*, vol. 69, pp. 107–111, 08 1991.
- [53] W. J. McComas and A. K. Bhattacharya, *Inquiry into Physics*. Pearson Prentice Hall, 6th ed., 2005.
- [54] M. Hegg and A. Maminshev, “Influence of variable plate separation on fringing electric fields in parallel-plate capacitors,” in *Conference Record of the 2004 IEEE International Symposium on Electrical Insulation*, pp. 384–387, 2004.
- [55] G. J. Sloggett, N. G. Barton, and S. J. Spencer, “Fringing fields in disc capacitors,” *Journal of Physics A: Mathematical and General*, vol. 19, p. 2725, oct 1986.
- [56] Pozzebon and Alessandro, “Bringing near field communication under water: short range data exchange in fresh and salt water,” in *2015 International EURASIP Workshop on RFID Technology (EURFID)*, pp. 152–156, 2015.
- [57] N. W. Bergmann, J. Juergens, L. Hou, Y. Wang, and J. Trevathan, “Wireless underwater power and data transfer,” in *38th Annual IEEE Conference on Local Computer Networks - Workshops*, pp. 104–107, 2013.
- [58] Epoxy Technology, “Understanding how to choose an appropriate thermally conductive epoxy.”
- [59] Total Materia, “Joining titanium,” 2005.
- [60] Nicolaas, “A blog about digital fabrication: The simplest slot joint,” 2015.

Appendix A

AI Use Screenshots

C can you explain the concept of using microwave radiation to measure salinity

🔊

❖ **Measuring Salinity with Microwave Radiation**

Microwave radiation is a type of electromagnetic wave with wavelengths ranging from about 1 millimeter to 1 meter. It's used in various applications, including telecommunications, radar, and, interestingly, **measuring salinity**.

How it Works

The key to measuring salinity with microwaves lies in how water molecules interact with this radiation. When microwave radiation passes through water, it interacts with the water molecules. The specific properties of this interaction, particularly the absorption and scattering of the radiation, depend on several factors, including:

- **Temperature:** Warmer water molecules absorb and scatter microwaves differently than colder ones.
- **Salinity:** The presence of dissolved salts in water can alter the way it interacts with microwaves.
- **Pressure:** The pressure of the water can also influence the interaction.

Salinity has a particularly significant impact on microwave interactions. The presence of dissolved salts can change the dielectric properties of the water, affecting how it absorbs and scatters microwave radiation. By carefully measuring these changes, scientists can infer the salinity of the water.

Figure A.1: AI Use for Concept Overviews

Applications

This technique has several applications, especially in oceanography and environmental science:

- **Ocean Salinity Profiling:** Scientists use microwave instruments mounted on satellites to measure the salinity of the ocean surface and even to profile salinity at different depths. This data helps us understand ocean circulation patterns, climate variability, and marine ecosystems.
- **Monitoring Coastal Waters:** Microwave sensors can monitor the salinity of coastal waters, which is crucial for understanding coastal ecosystems, managing fisheries, and protecting coastal communities from saltwater intrusion.
- **Studying Groundwater:** The salinity of groundwater can be measured using microwave techniques, providing insights into groundwater resources, pollution, and the interaction between surface and subsurface waters.

In essence, by understanding the relationship between microwave radiation and water properties, scientists can develop accurate and efficient methods for measuring salinity in various environments.

Figure A.2: AI Use for Concept Overviews

C

can you list all the methods that have been used to measure salinity throughout the past century



Methods Used to Measure Salinity Throughout the Past Century

Salinity measurement has evolved significantly over the past century, with advancements in technology leading to more precise and efficient methods. Here are some of the primary techniques that have been used:

Early Methods

- **Hydrometer:** A simple device that measures the density of a liquid. By comparing the density of seawater to that of pure water, salinity could be estimated.
- **Silver Nitrate Titration:** A chemical method involving the reaction of silver nitrate with chloride ions in seawater. The amount of silver nitrate used to react with all the chloride ions could be used to calculate salinity.

Mid-20th Century

- **Conductivity Meters:** These devices measure the electrical conductivity of seawater, which is directly related to its salinity. They were more accurate and easier to use than earlier methods.

Late 20th Century and Beyond

- **Salinity Sensors:** Continuous salinity measurements became possible with the development of electronic sensors that could be deployed in the ocean. These sensors were often combined with other oceanographic instruments to collect data over long periods.
- **Satellite Oceanography:** Satellites equipped with remote sensing instruments can measure the sea surface salinity from space. This technology has revolutionized oceanography, providing global coverage and frequent observations.
- **Autonomous Underwater Vehicles (AUVs):** These unmanned vehicles can be equipped with salinity sensors and other instruments to collect data at various depths in the ocean. They have been used to explore regions that were previously difficult to access.

Figure A.3: AI Use for Research Overview

C

ok can you add satellite-based measurements and evaporation to the list and then order it in chronological order

Show drafts ▾



◆ Salinity Measurement Methods in Chronological Order

Here's a revised list incorporating satellite-based measurements and evaporation, arranged chronologically:

1. **Hydrometry:** One of the earliest methods, using a hydrometer to measure the density of seawater.
2. **Chemical analysis:** Techniques like titration were used to determine salinity based on ion concentrations.
3. **Conductivity:** The invention of conductivity meters provided a more accurate and efficient way to measure salinity.
4. **Density:** While not as direct as conductivity, measuring density can still be used to estimate salinity.
5. **Microwave frequency:** This method utilizes the interaction of microwaves with seawater to determine salinity.
6. **Satellite-based measurements:** The advent of satellites equipped with remote sensing instruments allowed for large-scale, global salinity monitoring.
7. **Interferometry:** This technique uses the interference patterns of electromagnetic waves to measure salinity.
8. **Electromagnetic induction:** This method measures conductivity by inducing currents in seawater.
9. **Refractive index:** The refractive index of seawater can be used to infer salinity.
10. **Evaporation:** While not a direct measurement method, evaporation can affect salinity, especially in enclosed bodies of water.

Figure A.4: AI Use for Research Overview

C when using the `\cite[]()` command in latex, what can go in the square brackets

Show drafts ▾ 🔊

◆ The square brackets in the `\cite[]()` command in LaTeX are used to specify the citation style or to add additional information about the citation.

Here's a breakdown of what can go inside the brackets:

1. Citation Style:

- **Empty brackets:** If the brackets are empty, LaTeX will use the default citation style defined in your document preamble.
- **Style name:** You can specify a specific citation style by placing its name within the brackets. For example, `\cite[bibtex]{author2023}` would use the BibTeX style.

2. Additional Information:

- **Page numbers:** You can specify the page numbers where the citation appears:
`\cite[p. 23]{author2023}`.
- **Chapter or section numbers:** If the citation is from a specific chapter or section, you can include those numbers: `\cite[ch. 3]{author2023}`.
- **Notes or comments:** You can add notes or comments to the citation:
`\cite[Note: This is a controversial claim]{author2023}`.

Figure A.5: AI Use for L^AT_EX commands and code

```
% chktex-file 44
\begin{table}
\begin{tabularx}{\textwidth}{|C|C|C|C|C|C|}
\hline
\textbf{\$i\$} & \textbf{\$a\$} & \textbf{\$b\$} & \textbf{\$c\$} & \textbf{\$d\$} & \textbf{\$e\$} \\
\hline
\$0\$ & \$0.0080\$ & \$0.0005\$ & \$6.766097\text{e}\{-1\}\$ & & \\
\hline
\$1\$ & \text{\$-0.1692\$} & \$0.0056\$ & \$2.00564\text{e}\{-2\}\$ & \$3.426\text{e}\{-2\}\$ & \$2.070\text{e}\{-5\}\$ \\
\hline

```

Figure A.6: AI Use for L^AT_EX commands and code

C can you find a link explaining the IES-80 equations

Show drafts ▾ 🔍

◆ The International Hydrographic Organization (IHO) has provided a comprehensive document explaining the IES-80 equations. You can find it on their website:

International Hydrographic Organization (IHO) Standard Equation of Salinity - IES-80

https://iho.int/mtg_docs/IHReview/2017/IHR_May2017.pdf

This document provides detailed information on the mathematical formulas, algorithms, and procedures used to calculate salinity from conductivity, temperature, and pressure. It is a valuable resource for anyone working with oceanographic data and needing to understand the relationship between conductivity and salinity.

⬇️ ⏪ ⏴ ⏵ ⌂ ⋮

Figure A.7: AI Use for BibTeX citations

C can you turn this citations into bibtex
The Oceans, Their Physics, Chemistry, and General Biology. New York: Prentice-Hall, c1942 1942. <http://ark.cdlib.org/ark:/13030/kt167nb66r/>

Show drafts ▾ 🔍

◆ Absolutely, here's the BibTeX entry for the citation you provided:

Code snippet

```
@book{the_oceans,
    title = {The Oceans, Their Physics, Chemistry, and General Biology},
    author = {},
    % Since author is not available
    year = {1942},
    publisher = {Prentice-Hall},
    address = {New York},
    url = {http://ark.cdlib.org/ark:/13030/kt167nb66r/}
```

Use code [with caution](#). □

Figure A.8: AI Use for BibTeX citations

Appendix B

Graduate Attribute Assessment

Table B.1: Graduate Attribute Assessment

GA	Requirement	Justification and section in the report
1	Problem-solving	This project solved the problem of designing a compact salinity meter which included circuit, PCB and board-to-board communication design and embedded C coding in Chapter 4 .
4	Investigations, experiments and data analysis	This project investigating the properties of saltwater conductivity measurements and evaluated the performance of the probe in Chapter 6 .
5	Use of engineering tools	This project used KiCad software to design and fabricate PCBs , FreeCAD and PrusaSlicer to 3D print switch caps, and Microsoft Excel and MATLAB to conduct data analysis in Chapter 4 , 5 and 6 respectively.
6	Professional and technical communication	This project demonstrated professional and technical communication through the writing of a report covering the project.
8	Individual work	This report covers the individual report conducted by its author in the research, design, implementation and testing of a prototype salinometer in Chapter 2 , 4 , 5 and 6 respectively.
9	Independent learning ability	This report demonstrates the independent learning ability its author through the research in Chapter 2 conducted and applied to the design of a salinometer in addition to the iterative testing conducted in Chapter 6 .

Appendix C

Git Repository

[Link](#)

Table C.1: Git Repository Contents

Folder	Contents
PCBs	The design of the probe, controller and gold electrode PCBs .
Code	The code for the probe and controller PCBs and the communication between them.
Report	The LATEX code for this report.
Report Helper Documents	Files for creating graphs and images for this report and storing the results of the tests conducted.
CAD	The files for the switch caps.
GA Forms	The forms for submitting the graduate attribute assessment.